HADLEY CENTRE TECHNICAL NOTE NO. 10

THE IMPACT OF NEW PHYSICAL PARAMETRIZATIONS IN THE HADLEY CENTRE CLIMATE MODEL - HadAM3

By

V.D.Pope, M.L.Gallani, P.R.Rowntree and R.A. Stratton

Revised May 99

Climate Dynamics, to appear

August 1999

Hadley Centre for Climate Prediction and Research
Meteorological Office
London Road
Bracknell
Berkshire RG12 2SY

Abstract

Results are presented from the latest version of the Hadley Centre climate model, HadAM3 (Hadley Centre Atmospheric Model version 3). It represents a significant improvement over the previous version, HadAM2b. This is demonstrated using a series of ten year integrations with AMIP (Atmospheric Model Intercomparison Project) boundary conditions. The paper covers three aspects of model performance: (1) It shows the improvements in the mean climate in changing from HadAM2b to HadAM3. (2) It demonstrates that the model now compares well with observations. (3) It isolates the impacts of new physical parametrizations.

1 Introduction

General Circulation Models (GCMs) of the atmosphere are usually developed with either climate modelling or weather forecasting as their main use. The UK Meteorological Office (UKMO) Unified Model (Cullen, 1993) has been developed with equal emphasis on both. Climate modelling requires the best possible representation of the underlying physics, designed to minimise systematic errors in current climate and to represent physical processes as realistically as possible (this is particularly important for climate change studies). Weather forecasting, on the other hand, places the emphasis on reducing systematic errors in short-term forecasts. While these demands may at first sight appear conflicting they are often complementary, as systematic errors in the two versions of the model are often remarkably similar. An important attribute of GCMs is that they should be continually adaptable to changing requirements and improved physics. The UKMO Unified Model has been designed to make this as straightforward as possible. This paper describes the atmospheric component of the latest climate version of the model, which incorporates significant improvements to the physical parametrizations in the model and some major new features important for representing climate and climate change.

Many centres have developed GCMs for studying climate. Isolating the causes of differences between simulations with different models is difficult because they use a wide range of formulations. For example many use spectral discretisation, others use grid points, some use Eulerian and others semi-Lagrangian dynamics. They also use different physical parametrization schemes and often use different experimental design. The first attempt at a systematic comparison of a wide range of models was made in AMIP (the Atmospheric Model Intercomparison Project, Gates, 1992). This followed on from the more limited comparison made by Boer et al. (1992). AMIP provided a consistent method of assessing atmospheric climate models by providing an experimental design, including a specified integration time and standard boundary conditions. It has become the standard against which new models are assessed. The results presented in this paper all use the AMIP experimental design.

The first climate version of the UKMO Unified Model, HadAM1 (the Hadley Centre Atmospheric Model version 1), was used in AMIP. HadAM1 compared favourably with the wide range of climate models in AMIP (see for example Gates et al., 1999) and the earlier models analysed by Boer et al. (1992). For example HadAM1 had one of the smallest errors in multivariate statistics of mean sea level pressure. The next version of the Hadley Centre model, HadAM2, included very few changes and was used extensively in coupled mode, HadCM2 (Johns et al., 1997, C stands for Coupled). Changes in the atmospheric parametrizations were made in HadAM2b. Stratton (1999) used this version to study the effect on model results of changing horizontal resolution. Our paper compares and contrasts the latest version of the model, HadAM3, with HadAM2b. HadAM3 is the version being used in the follow- up to AMIP, AMIP II, and represents a significant improvement over previous versions submitted to AMIP. HadAM3 is also being used in a series of coupled ocean/atmosphere climate simulations, HadCM3 (Gordon et al., 1999).

The new model includes the following major changes to the physical parametrizations:
(1) A new radiation scheme (Edwards and Slingo, 1996).
(2) Convective momentum transport (Gregory et al., 1997).
(3) A new land surface scheme, MOSES (Met. Office Surface Exchange Scheme, Cox et al., 1999).
The model also has the following new capabilities important for climate research:
(a) It includes the radiative effects of aerosols and trace gases.
(b) It includes the effects of CO_2 on evaporation at the land surface.

One of the major aims of this paper is to isolate the impacts of the new physical parametrizations in HadAM3. This will help other climate modellers to decide whether similar improvements could help reduce systematic errors in their own models. Therefore, as well as describing the improvements in model climate in HadAM3 and the remaining absolute errors relative to observational analyses we also investigate the physical mechanisms for the changes in model climate using three methods.

First, we make use of a comprehensive series of AMIP runs (using the 10-year AMIP I boundary conditions) which test all parametrization changes to the model individually. From these we can associate some of the individual changes in model climate with individual changes in parametrizations. This is not always straightforward since the parametrization changes interact with one another and therefore do not add linearly. Even where associations can be made, the link between climate and parametrization changes may not always be direct. For example, convective momentum transport has a large direct impact on winds in the tropics, which alters the global circulation producing indirect impacts on the extra-tropical circulation.

Second, we examine the increments (or 'tendencies') in the basic model variables made by individual model schemes, in order to distinguish between the direct and indirect impacts of parametrization changes. The tendencies are shown for the first 10 days of the AMIP integrations (starting from analyses). These often show that the model mean errors are already being established by model drift early on in the integration - hence, the consistency between climate and forecast errors pointed out above.

Third, the impact of the new radiation scheme is examined in further detail using calculations with the HadAM3 radiation scheme made using HadAM2b model fields. This allows us to isolate radiative feedbacks.

The paper is organised as follows. Section 2 is a description of the basic Hadley Centre model highlighting the differences between HadAM2b and HadAM3. Section 3 contains a brief summary of the main climatologies used to evaluate the model. Section 4 is a comparison of HadAM2b and HadAM3 and an evaluation of the model against relevant climatologies. Section 5 is a detailed assessment of the impact of the new Edwards-Slingo radiation scheme on the model's mean climate. Section 6 is an assessment of the other model changes on the model's mean climate. Finally, the discussion and conclusions are in section 7.

2 Model description

2.1 Basic features of the model

HadAM3 is based on the previous version of the climate model HadAM2b, described by Stratton (1999), with some major improvements. The basic features of both versions of the model are as follows.

2.1.1 Dynamics
The current Unified Model (Cullen, 1993) is a hydrostatic, grid point model using an Arakawa B grid and hybrid vertical co-ordinates. It uses an Eulerian advection scheme. Both HadAM2b and HadAM3 use a 2.5° latitude by 3.75° longitude grid and 19 model levels, and a 30-minute timestep.

2.1.2 Cloud scheme
The model uses a prognostic cloud scheme, described by Smith (1990) and modified by Gregory and Morris (1996), which diagnoses cloud ice, cloud water and cloud amount from the primary model variables q_T (total moisture) and liquid water potential temperature.

2.1.3 Precipitation
The model uses the precipitation scheme described by Senior and Mitchell (1993) together with the evaporation of precipitation described by Gregory (1995).

2.1.4 Convection
Moist and dry convection are modelled using the mass-flux scheme of Gregory and Rowntree (1990) with the addition of convective downdrafts (Gregory and Allen, 1991).

2.1.5 Gravity-wave drag
The parametrization of sub-grid scale orographic gravity-wave drag is that of Gregory et al (1998).

2.1.6 Boundary layer
Both models use the scheme developed by Smith (1990, 1993).

2.2 Main differences between HadAM2b and HadAM3

2.2.1 Radiation
HadAM2b used the scheme described by Slingo (1989) and Slingo and Wilderspin (1986). This has 4 shortwave bands and 6 longwave bands. It includes the effects of CO_2, H_20, and O_3. HadAM3 uses the new radiation scheme developed by Edwards and Slingo (1996) and modified by Cusack et al. (1999). This has 6 shortwave bands and 8 longwave bands. As well as including the effects of CO_2, H_20, and O_3 it also includes the effects of O_2, N_20, CH_4, CFC11 and CFC12. The model uses trace gas values appropriate for the AMIP I period, i.e. 1979-1988. HadAM3 also includes the developments made by Cusack et al. (1998) to include the effects of background aerosols. Further improvements in HadAM3 are that ice crystals and water droplets are treated separately in the radiation scheme. Cloud overlaps are treated consistently in the shortwave and the longwave regions: in particular, layer cloud in the shortwave is no longer reduced to three layers.

2.2.2 Convective momentum transport
The direct impact of convection on momentum was not included in HadAM2b. The effects are included in HadAM3 using the scheme developed by Gregory et al. (1997).

2.2.3 Land surface scheme
HadAM2b uses the scheme described in Lean and Rowntree (1997). HadAM3 includes MOSES, the new land surface scheme developed by Cox et al. (1999). The new land surface scheme includes a representation of the freezing and melting of soil moisture leading to better simulations of surface temperatures, and a new formulation of evaporation which includes the dependence of stomatal resistance on temperature, vapour pressure deficit and CO_2.

2.3 More minor differences

2.3.1 Critical relative humidity (RH_{crit})
In the Smith cloud scheme cloud cover and cloud condensed water amount within a grid box are predicted using a specified distribution of total water content within the grid box. The standard deviation of this distribution is related to a critical relative humidity (RH_{crit}) below which no cloud forms. There is some uncertainty over the precise value that RH_{crit} should take, indeed there is some evidence that the value used in HadAM2b (0.85 at all levels above level 3) is too large in some parts of the troposphere. Therefore, in HadAM3 RH_{crit} is reduced to 0.7 above level 3. This value was chosen to maintain a global mean radiation balance close to zero at the top of the atmosphere in a pre-industrial simulation with the coupled model. This helps to avoid climate drift in the control simulation. Reducing RH_{crit} tends to increase the amount of water cloud and decrease the amount of ice cloud. Note that the standard deviation of the probability density function changes as well as the critical humidity at which cloud starts to form, so the impact of changing RH_{crit} depends on how saturated the grid box is.

2.3.2 Boundary layer mixing and convection
In HadAM2b, the boundary layer scheme consists of a local mixing scheme. This uses a mixing coefficient, which is a function of a mixing length, the local wind shear and atmospheric stability. It also includes a representation of non-local mixing (rapidly-mixing scheme; Smith 1993) which uniformly distributes the heating and moistening resulting from the divergence of the fluxes between the surface and the top of the boundary layer. The rapidly-mixing scheme was included because, in

unstable regions, the fluxes are in fact not closely related to the local gradients. Also, the local values of stability can be influenced by other parts of the model, particularly the convection scheme, thereby altering the turbulent mixing unrealistically. However, during the development of HadAM3, it was found that the rapidly-mixing scheme produced unfavourable interactions with the transport and sink of aerosols. Therefore, the rapidly-mixing scheme is switched off in HadAM3. In addition, the mixing length is reduced above the diagnosed top of the boundary layer and increased in the mixed layer. Also, the amount of freezing and melting of convective precipitation which is not falling through downdraughts is limited so that the temperature change due to the phase change does not increase/decrease the temperature above or below the melting point of water.

2.3.3 Gravity-wave drag
Corrections were made to the new gravity wave drag scheme introduced into the model at HadAM2b. In HadAM2b the use of a critical stress level in the new scheme was being incorrectly applied resulting in some drag being applied too high in the atmosphere.

2.3.4 Cloud
The coefficient known as Cw (see equation 2.29 in Smith, 1990) which controls the rate at which cloud liquid water is converted to large-scale precipitation was reduced. In both HadAM2b and HadAM3 the coefficient Cw takes different values over land to those over the sea in an attempt to take account of the differences in cloud condensation nuclei. The values for the two versions of the model are as follows;

	over sea	over land
HadAM2b	2.0e-4	8.0e-4
HadAM3	0.5e-4	2.0e-4

A reduction in Cw increases the rate of conversion of cloud liquid water to precipitation.

2.3.5 Minor change affecting radiation
In HadAM3 the water vapour used by the radiation code has a lower limit of 2.5e-6 kg/kg. The actual water vapour of the model can fall below this value. In both HadAM2b and HadAM3 negative values are reset by borrowing from adjacent grid points.

2.3.6 Ozone
HadAM3 uses the Li and Shine (1995) climatology based on recent satellite measurements in the stratosphere and a limited set of ground based measurements in the troposphere. HadAM2b used the Keating et al. (1987) climatology for the top 2 levels (above 20 hPa) and McPeters et al. (1984) below (values below level 9, about 422 hPa, were equal to those at level 9).

3 Climatologies used for model evaluation

3.1 ECMWF reanalyses

We make extensive use of the ERA climatology (Gibson et al., 1997, Kallberg, 1997). The reanalysis climatologies are ideal for evaluating climate models for the AMIP period for the following reasons:
(1) They use the same analysis method throughout.
(2) They provide self-consistent fields.
(3) They cover the globe.
(4) They span the AMIP period.
(5) The ERA climatology has a particular advantage for humidity analyses since it assimilates satellite radiances. McNally and Vesperini (1996) show that this method produces realistic humidity analyses that are not strongly dependent on the characteristics of the GCM used.

The reanalysis data have certain pitfalls. First, the large variation in the accuracy and range of observation types in different regions is not obvious in the analysed fields. In northern mid latitudes over land, radiosonde and aircraft measurements are combined and supplemented with satellite measurements to give accurate analyses. Elsewhere there are fewer observations, and in some regions satellite observations may be the only source of information. Whilst satellite radiances can be assimilated into models to provide reasonable estimates of atmospheric temperature and (less accurately) humidity they are of limited use, particularly in providing surface variables. Also, some

fields are poorly represented. For example fields that are not measured directly, such as cloud water, will be dominated by model biases. There are some known errors in the ERA dataset. The most serious is the drying of the soil in Amazonia. Another error led to the soil temperatures during winter and spring being too low over frozen and snow-covered high latitudes. This fed back into too cold atmospheric boundary layers. In some regions the analysis may be dominated by the model behaviour. Obvious areas are sparsely populated ones such as the polar regions and large oceans.

We have made a cursory comparison of the ERA and NCEP-NCAR climatologies and found that the differences between the climatologies in a basic field such as temperature are often as much as the differences between the model and the closest climatology.

3.2 Other datasets used

3.2.1 CMAP
Precipitation is evaluated against the CPC Merged Analysis of Precipitation (CMAP, Xie and Arkin, 1997). This is a global, monthly precipitation dataset covering the 17-year period 1979 to 1995. It incorporates gauge observations, estimates inferred from a variety of satellite observations and the NCEP-NCAR reanalysis (Kalnay et al., 1995).

3.2.2 ERBE
Satellite measurements of radiative fluxes made between 1985 and 1990 by ERBE (Harrison et al., 1990) are used to evaluate the model's radiation fluxes at the top of the atmosphere.

3.2.3 Legates and Willmott
1.5 m temperatures over land are evaluated against the Legates and Willmott climatology (1990). This is based on observations for the period 1920-1980.

4 Mean fields

Most of the fields shown are 10 year seasonal means. We concentrate on djf (December to February) but show or describe other seasons where there are significantly different results.

4.1 PMSL and 500 hPa height

The pressure at mean sea level (PMSL, Fig. 1) is improved in most regions in HadAM3. An exception is the tropics where the low pressure bias is increased. Similar changes are found in 500 hPa height, indicating that the PMSL changes are characteristic of the whole lower troposphere. Globally, the total improvement in rms. error is of order 15%. Biases over the NE Pacific, N America, N Atlantic and N Eurasia are reduced during northern winter (Fig. 1) and spring (not shown). The increases in pressure over the N Pacific and N Atlantic are consistent with increased blocking (see below). The local low pressure bias in the Atlantic in HadAM2b meant that the westerly winds were shifted too far south (see pressure gradients in Fig. 1(c)). This error has been removed in HadAM3, but there is still a general high pressure bias at high latitudes resulting in a bias in the pressure gradients consistent with an easterly bias in the low level winds (Fig. 1(d)). The wind stresses at the ocean surface are therefore too weak in the N. Atlantic storm track (Gordon et al., 1999).

PMSL is generally higher over Antarctica in HadAM3, giving large reductions in the rms. errors for the southern hemisphere, averaging 25%. The changes in pressure are also associated with a decrease in the excessive westerly winds over the southern ocean. The change in pressure gradients at 50 S in Fig. 1 give some indication of this, although the impact is much larger during southern winter (not shown). This gives a significant improvement in the surface stresses over the southern ocean. Gordon et al. (1999) show that these now compare very favourably with observations.

It is also important to evaluate the variability of the circulation. One measure of this is the frequency of occurrence of blocking. The blocking index (defined by Tibaldi and Molteni, 1990) for

northern hemisphere winter is shown in Fig. 2. In HadAM2b there is virtually no blocking over the Pacific and there is unrealistic blocking in the west Atlantic. In contrast in HadAM3 the blocking in the Pacific has realistic amplitude and extent and there is no spurious peak in the west Atlantic. These improvements (particularly in the Pacific) may be associated with improvements in the Indonesian precipitation and circulation in HadAM3 (see section 4.4). A number of studies (including Ferranti et al., 1994) have shown that improved diabatic forcing over Indonesia can result in increased blocking in the Pacific and (less conclusively) improved blocking in the Atlantic.

The main systematic errors in HadAM3 are now high pressure at high latitudes for most of the year, affecting both the pole and the Icelandic low in the northern hemisphere. Associated with these biases are easterly biases in the surface winds.

4.2 Winds

4.2.1 Zonal-mean zonal wind

The zonal mean zonal wind (u, Fig. 3) is considerably improved in HadAM3. This improvement comes almost entirely from the inclusion of the convective momentum transport. The improvements are particularly striking in the tropics, where the westerly bias in the mid troposphere is removed and the easterly bias around the tropopause is halved. There are also reductions in the westerly bias at mid latitudes and the easterly bias at high latitudes, mainly in the winter hemisphere. There is still a large westerly bias in the southern hemisphere and the stratospheric jet is too far equatorward in the northern hemisphere.

4.2.2 Mean meridional circulation

The mean meridional wind is illustrated in Fig. 4. The northward flow in the upper branch of the Hadley circulation is shifted downwards, which is an improvement, but it is now too strong. The associated vertical motion is too strong in both models, but the vertical extent of the error is reduced in HadAM3. The downward shift in the Hadley circulation is probably associated with the reduction in the depth of convection (section 4.4.2). In the lower troposphere there is increased southward flow into the ITCZ, increasing convergence. There is correspondingly more ascent in this region (not shown) and stronger divergence in the upper troposphere (Fig. 5 below).

4.2.3 Divergent winds

Fig. 5 shows the velocity potentials at 200 hPa (the gradient of velocity potential is proportional to the divergent flow). We show the absolute fields rather than differences as it is the gradients that are important and not differences in the values. The main regions of divergence and convergence coincide with the main convectively active and inactive regions. Increased convective activity is associated with increased precipitation, decreased OLR and increased divergence (see below).

In djf, the structure of the divergent wind is improved, but its strength is increased too much (the Hadley and Walker circulations are too strong). In particular, the structure is improved over Indonesia; notice the orientation and shape of the strong gradients. The improved structure is associated with significant changes in the precipitation and OLR (see below). In other regions and in jja (June to August, not shown) the changes are dominated by the increase in strength of the divergent circulation. The change is particularly large because we are showing a single level and the Hadley circulation has shifted down, weakening at 150 hPa and strengthening at 200 hPa.

4.3 Temperature

The temperature biases are substantially reduced in HadAM3. Most of the changes arise from the inclusion of the new radiation scheme (see section 5). Fig. 6 shows the mean temperatures for djf. The cold bias in the troposphere is significantly reduced, particularly in the upper troposphere, at the tropopause and in the tropics. Although the temperature changes at high latitudes are quite large the cold biases are still significant. In the lower troposphere at high northern

latitudes the cold bias is worse in HadAM3. The warm bias in the stratosphere is removed, with some levels now too cold (again due to changes in the radiation scheme).

4.4 Moisture and cloud

4.4.1 Relative and specific humidity

Most aspects of the moisture fields are improved in HadAM3. Figs. 7 and 8 show the relative and specific humidity (comparisons with ERA are only shown for relative humidity because this is the analysed field). In the upper troposphere the specific humidity is higher since the warmer air can hold more moisture. However, the increase is not large enough to balance the temperature changes and the relative humidity is lower. The stratosphere is much drier in HadAM3 - at some levels there is almost no moisture. This arises from the poor representation of water vapour transport due to the crude vertical resolution using 19 levels. There is no obvious reason why HadAM3 should be worse than HadAM2b. Indeed, the warmer tropical tropopause should mean that the air entering the stratosphere is moister. The only region where both the relative and specific humidity show an increase in moisture is in the tropical middle troposphere.

Overall, despite the improvements in the moisture distribution, there is still a large moist bias, particularly in the winter storm track and at high latitudes in summer.

4.4.2 Cloud amounts

The troposphere is more stable in HadAM3 and there is correspondingly weaker convection and less convective cloud (Fig. 9, no direct comparison with observations is possible since only total cloud is observed). In HadAM3 convection is initiated higher up (note the decrease in low level cloud) and is not as deep (decrease in high level cloud). The convective heating rates (not shown) also demonstrate the overall decreased convective activity. The convection deposits moisture lower in the atmosphere - hence the increased relative humidity in the middle troposphere (section 4.4.1).

This description gives a broad picture of the differences between convection in HadAM3 and HadAM2b. However, there are some more subtle effects worth pointing out. The link between convective cloud and convection is not linear. The instantaneous convective cloud amount is proportional to the log of the instantaneous precipitation. The mean cloud amount is the accumulation of these instantaneous values. The nonlinearity is particularly striking in the Indonesian region where convective precipitation increases markedly with very little change in convective cloud amount. Analysis of the cloud amount and precipitation timestep by timestep shows that in this region the convection is more intermittent, but stronger when it does occur, in HadAM3.

Changes in layer cloud are shown in Fig. 10. They are dominated by decreases in most regions, and in particular in the upper troposphere. The only exception is the tropical lower to middle troposphere where there is more cloud. These changes are consistent with the changes in relative humidity, with cloud forming more (less) readily where relative humidity has increased (decreased). There is also an increase and downward shift in the layer cloud in the boundary layer in the summer hemisphere, occurring mainly over the sea, improving agreement with the climatology in Warren et al. (1988) which has fog in these regions. This feature is more prominent in northern summer than in southern summer, which is why we show jja (June to August) for this field rather than djf. The air in this region is close to saturation near the surface in both versions of the model. A small change in temperature structure is associated with decreased convection in the lower troposphere (not shown). Cloud then forms more readily in the lowest layers of the model.

The overall effect of these changes is to decrease cloudiness nearly everywhere. There is a corresponding decrease in shortwave radiative cloud forcing (see section 5.2) everywhere except the tropics (where layer cloud increases in the middle troposphere).

4.5 Precipitation and Outgoing Longwave Radiation

Changes in the global distribution of precipitation are shown in Fig. 11. The rms. errors in precipitation for different versions of the model are quantified for different latitude bands over land and sea in Fig. 12. We have included comparisons over the sea, although the data are not as reliable as land data. In the northern extratropics HadAM3 is generally drier than HadAM2b and rms. errors are reduced. However, there is still more precipitation than the CMAP dataset suggests.

In the tropics, Fig. 11 shows that there is less precipitation over most regions. Fig. 12 shows that this increases rms. errors over land but decreases them over the sea. In djf, Fig. 11 shows that there are increases in precipitation over the Indonesian region and decreases to the east and west leading to local reductions in the model biases. The annual mean rms. error over Indonesia decreases by 6%. The associated divergent flow (section 4.2.3) and Outgoing Longwave Radiation (see below) also improve in this region. There are increased rms. errors in precipitation over tropical America (20%) and Africa/India (10%). The change over the Africa/India region, arises from degradations in the monsoon circulation (see Martin and Soman, 1999, for more details). There is a tendency for the seasonal shifts in African and Asian tropical rainfall to occur earlier and be more marked in HadAM3, leading to increased rms. errors in September to November and March to May.

Globally, mean changes in precipitation are small over land with rms. errors increasing slightly. There is a systematic decrease in mean precipitation in all parts of the globe over the sea, reducing rms. errors by over 20%.

Outgoing Longwave Radiation (OLR) is often used as a proxy for precipitation. Increases in deep convective cloud are associated with increases in precipitation. The additional cloud traps more longwave radiation in the atmosphere so reducing the OLR. This relationship is particularly useful where precipitation observations are sparse, such as over the ocean, since OLR can be obtained from satellite datasets such as ERBE. There is an added complication in comparing HadAM3 and HadAM2b because the OLR changes partly as a direct result of using a different radiation scheme (see section 5). Fig. 13 shows the OLR for djf. The main changes in OLR are anticorrelated with the changes in precipitation, as we would expect. The most striking improvement is over Indonesia, where the OLR is reduced by 20 Wm^{-2} over a large region coinciding with increases in precipitation. This is one of the most difficult tropical convective regions to model. HadAM3 shows a substantial improvement in the representation of precipitation, OLR and divergent flow here, due in large part to the inclusion of convective momentum transport and the new radiation scheme.

4.6 Surface fields

4.6.1 Surface temperatures

Globally, both HadAM2b and HadAM3 are too cold near the surface. This is illustrated in maps of 1.5m temperatures for djf in Fig. 14, and in a bar chart of mean and rms. errors over land for different regions and seasons in Fig. 15. Note that we focus on land only, since the temperatures will be strongly constrained by the prescribed SST over the sea. Fig. 14 oncludes all land points outside Antarctica, although we do not place much weight on mountainous regions because of the problems of relating observations and model data in these regions (e.g. note that the differences are off the end of the colour scale over the Himalayas). Fig. 15 excludes all points above 1500m. The global mean cold bias is reduced by 0.3K in the annual mean in HadAM3 when compared to HadAM2b. The tropics share in the global cold bias and its reduction in HadAM3. The rms. errors also decrease in HadAM3, though only slightly in the tropics.

The largest cold biases are in the northern hemisphere during winter. The strength of the cold bias in different regions (Fig. 14) is modulated by the errors in low level advection evident from the pmsl (Fig. 1). Over northern Eurasia there is an easterly bias (reducing the advection of warm air off the Atlantic over the continent) and the cold bias is particularly large. Over N America there is a southerly bias and temperature bias is relatively small. On the eastern side of the continent there is even a warm bias. These wind biases are reduced in HadAM3 as compared to HadAM2b and the contrast in temperature errors is correspondingly reduced. The cold bias over Eurasia is reduced and

the small warm bias over eastern N America changes to a small cold bias. The errors in the extra-tropics show a strong seasonal variation (Fig. 15) with maximum mean and rms. errors in winter, when parts of the northern continents are too cold by over 10K, and minimum errors in summer (discounting Antarctica where there is little data). This seasonal variation is exaggerated in HadAM3 in both hemispheres.

4.6.2 Surface fluxes

A major aim of the development of HadAM3 was to reduce the surface flux errors over the ocean so that the coupled model could be run without the need for flux adjustments. Validation of the success of this effort is hindered by the poor quality of observational estimates of the ocean surface fluxes. This applies to all the component fluxes: turbulent heat and moisture fluxes, longwave and shortwave radiative fluxes, precipitation. For example, the mean error in the net ocean surface heat flux is about 30 W m^{-2} in the da Silva analyses (1994). The solar flux is particularly suspect, as it is derived using a numerical model.

The validation here is therefore mainly restricted to an analysis of the changes in the net heat fluxes over regions where the coupled model exhibited large errors when run with HadAM2b. Fig. 16 shows the net ocean surface heat fluxes into the ocean in selected regions in HadAM2b and HadAM3. It turns out that negative (positive) net heat fluxes are often correlated with negative (positive) sea surface temperature errors when the model is run in coupled mode without flux adjustment. In nearly all cases (except the Arctic and W Pacific) net surface heat fluxes are numerically smaller and corresponding SST errors in the coupled model (Gordon et al., 1999) are smaller in HadAM3 than in HadAM2b. The coupled model is particularly sensitive to the net cooling of the ocean surface in the northern oceans (NW Atlantic, NE, NW and E Pacific) associated with excessive latent heat flux out of the ocean. It is also sensitive to the net warming in the southern ocean associated with excessive downward shortwave heating where there is too little cloud overhead. Even though each of these fluxes is numerically reduced in HadAM3 the sea surface temperatures in the coupled model suggest the fluxes are still excessive. In the tropics there is a large positive net heat flux associated with excessive solar heating. In the Indonesian region (Eq. W Pacific) this is associated with the lack of cloud and rain (section 4.5) and in the marine stratocumulus regions (Eq E Pacific and Eq E Atlantic) with a lack of cloud. All of these errors are reduced in HadAM3 and the net surface heat fluxes are correspondingly reduced.

5 Impact of the Edwards-Slingo radiation scheme on the model climate

In this section we make use of additional model runs to assess the impact of the new radiation scheme (R):
1. A parallel integration of HadAM3, identified as HadAM3-R (i.e. HadAM3 minus R), which uses the HadAM2b radiation scheme.
2. Spin-up runs of HadAM3 and HadAM3-R for 10 days from the beginning of December to identify the changes in heating rates from the individual model schemes when R is included in the model. This gives us information on how the individual schemes respond to the new radiation scheme.
3. A 'double call' test of the radiation (provided by John Edwards). One December-February season of HadAM2b was repeated with R (including the effects of aerosol) run alongside the HadAM2b radiation scheme. R was used to provide radiation diagnostics but did not feed back on the model fields. This allows us to assess the direct impact of R on the temperatures excluding any feedbacks.

5.1 Temperature

The direct effect of changing the radiation scheme is to alter the temperatures. Fig. 17 shows the change in the mean temperature when the HadAM2b radiation scheme is replaced with R (panel (a)). It also shows the change in the total heating rate from all the model schemes over the first 10 days of the integration (panel (b)) together with the change in the heating rates from the shortwave and longwave radiation schemes (panels (c) and (d)). Panels (a) and (b) show that change in the spin-up heating rate qualitatively accounts for the change in mean temperature, in that there is relative warming in the troposphere, cooling in the lower stratosphere and warming in the middle stratosphere with R. Comparison with Fig. 6(b) shows that R is the main contributor to the

differences in temperature between HadAM2b and HadAM3. The changes in net heating (panel (b)) are dominated by the changes in shortwave and longwave heating (panels (c) and (d)). The differences in heating rates are partly the direct effect of R and partly indirect effects due to changes in the temperature, moisture and cloud fields.

To identify the direct effects of R, Fig. 18 shows the differences between the temperature tendencies in the double call test; i.e. R - non R calculated from HadAM2b model fields. The shortwave heating is increased through most of the troposphere due to changes in the clear-sky fluxes (panel (c). Absorption by aerosol, included in R, contributes to this. Near the tropical tropopause the shortwave heating is decreased due to changes in the cloudy fluxes (the difference between Fig. 18(a) and Fig. 18(c)). In the old radiation scheme all the shortwave absorption in convective cloud was at the top of the cloud. The new treatment is more realistic, significantly reducing the local maximum absorption at the cloud top. A smaller but significant reduction in shortwave absorption comes from the indirect effect of reducing the amount of cloud (see below)

Changes in longwave cooling are dominated by changes in clear-sky effects except at the tropopause (compare Figs. 18 (b) and (d)). Note for example the reduction in cooling (i.e. positive differences) in the lower and upper troposphere (particularly in the tropics) which contributes to the reduction of the cold bias in HadAM3. The reduction in cooling in the lower troposphere arises mainly from the use of the CKD continuum model (Clough et al., 1989) instead of the RSB model (Roberts et al., 1976). The changes above Eta=0.25 arise mainly from changes in the treatment of carbon dioxide and ozone. The reduction in cooling is particularly pronounced in the bottom layer of the model. The heating rates adjust to the higher temperatures, however. Hence, the relative warming at low levels in Fig. 17(d) is much smaller than the corresponding warming in Fig. 18(b).

There are also changes in longwave cloud forcing (the difference between Fig. 18(b) and Fig. 18(d)). Changes in clear-sky absorption in the window region make the lower atmosphere more transmissive to longwave radiation. There is more upward flux into the cloud and consequently more warming of cloud in the upper troposphere (Eta=0.3-0.15). This effect is not particularly sensitive to the amount of cloud and is only reduced slightly by the reduction of cloud in HadAM3 (compare Figs. 17(d) and 18(b)). The net effect on cloud forcing at the top of the atmosphere (see section 5(b)) is small.

The new radiation scheme also impacts on surface temperature. Figure 15 shows the contribution of R (compare AM3-R and AM3) to the overall change from HadAM2b to HadAM3 for different regions of the globe. R reduces the surface cold bias, consistent with changes in downward radiative flux at the top of the atmosphere (R gives an increase of 5.5 Wm^{-2}, see below). MOSES (the new land surface scheme) also reduces the cold bias, but other changes increase it. These changes are necessary to bring the radiation back into balance at the top of the atmosphere. In most regions the temperature increases, and the mean and rms. errors reduce. In the southern hemisphere, however, the mean temperature decreases, and the mean and rms. errors increase. Note that Antarctica is not included in this comparison because of the lack of reliable observations, but comparison of the models indicates an increase in temperature. Over Antarctica the direct effects of R (Figs. 17 and 18) are cooling in the bottom layer, both from longwave clear-sky forcing and shortwave cloud forcing. This is more than compensated for by the indirect effect of changes in boundary layer heating; hence the net effect of including R in the model is to increase the surface temperature over Antarctica.

The indirect effects of R are generally small, i.e. Figs. 17(c) and 18(a) are very similar as are Figs. 17(d) and 18(b). The main exceptions are:
1. In the tropics, reduced shortwave heating in the upper troposphere and increased heating in the lower troposphere. This is consistent with the reduction of tropical cloud amounts (Figs. 9 and 10), absorbing less radiation in the upper troposphere and allowing more to reach lower levels.
2. The stratospheric cooling around Eta=.015 is much more marked in the double call test. This arises because of the way the two radiation schemes treat low water vapour values. R gives more longwave cooling because it uses a minimum water vapour value ($2.5x10^{-6}$ kg/kg) where the air is very dry. Hence there is a large difference in the response of the two radiation schemes at these levels. The cooling is less marked in HadAM3 than in the double call test because the temperatures can respond to the cooling, and the cooler atmosphere radiates less.

5.2 Radiation budget

There are significant differences between HadAM2b and HadAM3 in their global mean radiative balances. These are summarised in table 1. We discuss this here because most of the differences arise from the inclusion of the Edwards-Slingo radiation scheme. This is shown in the last column (impact R). The impact of all other changes to the physical parametrizations are shown in the 3rd column (impact non-R). The main impact is from the change to critical relative humidity (section 6.3).

The figures in table 1 are derived from the radiative fluxes from HadAM2b, HadAM3-R and HadAM3. In analysing the results we have also made use of an additional integration - namely an early test of HadAM2b+R (this version did not include aerosol, convective cloud overlaps and other more minor changes). This allows us to identify robust results that do not depend on interactions with other parametrization changes.

Table 1. Ten year annual mean global means at the Top Of the Atmosphere (TOA) (Wm^{-2}). Impact non-R is HadAM3-R - HadAM2b. Impact R is HadAM3 - HadAM3-R. Arrows indicate upward or downward fluxes. Other terms are defined in the text.

	HadAM2b	HadAM3	Impact non-R	Impact R
Clear sky OSW↑	47.0	51.6	0	4.6
SW cloud forcing↓	-51.9	-47.6	-2.5	6.8
OSW↑	98.9	99.2	2.5	-2.2
Clear sky OLR↑	264.1	259.9	-.3	-4
LW cloud forcing↓	23.7	21.1	-2	-.6
OLR↑	240.4	238.7	1.7	-3.4
TOA radiation↓	2.2	3.5	-4.2	5.5

The increased clear sky outgoing shortwave radiation (OSW) is almost entirely due to the inclusion of aerosol (Cusack et al., 1998). The decreases in the magnitude of the shortwave cloud forcing are consistent with the decreased cloud amounts discussed in section 5(a). The decreased absorption by cloud evident in Fig. 18(a) might be expected to be associated with decreased reflection decreasing the magnitude of the shortwave cloud forcing.

The outgoing longwave radiation (OLR) changes for a number of reasons in HadAM3. The introduction of new trace gases (CH_4,N_2O and CFC11 and 12) makes a significant contribution to the reduction in clear sky OLR. A large change of opposite sign comes from the improved treatment of the water vapour continuum in the calculation of clear sky fluxes. The atmosphere is effectively less opaque and so the in situ cooling is less (see above). This is consistent with a reduction in the downward flux at the surface (see the discussion in section 5(c)). We might expect the less opaque atmosphere to increase OLR at the Top Of the Atmosphere (TOA), whereas the opposite happens. Detailed calculations for different spectral bands (Edwards, personal communication) show that the decrease in OLR comes from wavenumbers greater than 1200 cm-1 where the treatment of the 2 radiation codes is very different (in the window region the OLR is higher with R, as we would expect). The clear-sky OLR is now low compared to ERBE and in purely numerical terms is not improved. However, since the model is both cold and moist a low clear-sky OLR should be expected.

5.3 Energy and moisture budget

In climatological equilibrium the atmospheric thermal energy budget is zero in the global annual mean. This constraint means that changes in the radiative heating in the model must be balanced by changes in the other heating terms. The global mean budget takes the following form:

Net radiative heating of the atmosphere + latent heat release + sensible heat from surface = 0

(Note that this equation omits the conversion from available potential energy to eddy kinetic energy and frictional heating. The model assumes they balance.)

Table 2. Ten year annual mean global mean atmospheric thermal energy budget (Wm^{-2}). The "observations" are derived from Kiehl and Trenberth (1997). It should be noted that they use models to infer the surface fluxes. Impact non-R is HadAM3-R - HadAM2b. Impact R is HadAM3 - HadAM3-R. Arrows indicate upward or downward fluxes. Other terms are defined in the text.

	HadAM2b	HadAM3	Obs. Est.	Impact non-R	Impact R
Sensible heat	20.5	16.7	24	-0.1	-3.7
Latent heat release	93.8	84.2	78	0	-9.6
Net radiation	-114.3	-100.9	-102	0.1	13.3
SW radiation	67.4	75.7	70	-0.2	8.5
LW radiation	-181.6	-176.5	-168	0.3	4.8

Radiative cooling of the atmosphere is balanced by latent heat release and sensible heat flux from the surface. The radiative cooling is reduced by 13.3 Wm^{-2} in HadAM3 due almost entirely to the new radiation scheme, giving significantly better agreement with observations. Note that there are considerable variations in observational estimates, however. The flux most likely to be in error is the ShortWave (SW) surface flux, since estimates vary by as much as 14 Wm^{-2}. A major contributor to the change in our model is the increased heating due to the inclusion of aerosols (5.5 Wm^{-2}, Cusack et al., 1998). Other contributions come from increased solar absorption in the stratosphere, and reduced clear-sky LongWave (LW) cooling in the lower and upper troposphere as outlined in section 5(b). The reduced radiative cooling of the atmosphere in HadAM3 is balanced by reduced latent heat release (also improving agreement with observations) and by reduced sensible heat flux from the surface.

The impact of the new radiation scheme on the downward ocean surface fluxes is shown in Fig. 19. The latent heat flux out of the ocean decreases everywhere (i.e. bars on the figure are positive) consistent with reduced latent heat release in the atmosphere (table 2). The net radiative heating of the surface is smaller (negative bars) consistent with the smaller radiative cooling of the atmosphere. The largest reductions are in the equatorial west Pacific, associated with a downward shift of layer cloud in this region (see below).

A substantial part of the reductions in relative humidity (Fig. 7) and cloud amounts (Figs. 9 and 10) in the upper troposphere in HadAM3 arise when R is included in the model, and are associated with increases in temperature. Convection is strongly affected when the new radiation scheme is included. Over land, R tends to warm the lowest layers including the surface (Fig. 15), enhancing convective instability. Over the sea, the contrast between warm sea and cooler air is reduced, reducing convective instability. This is reflected in increased precipitation over land in the tropics, in particular over Africa and Asia in jja and Indonesia in djf and decreased precipitation over the sea at all latitudes (Figs. 11 and 12). The monsoon circulation increases with the new radiation scheme (Martin and Soman, 1999) increasing precipitation over the western Pacific and over the Indian peninsula and decreasing it over the Indian Ocean. This degrades the monsoon simulation, although locally the increased precipitation over the western Pacific is an improvement.

In the zonal mean the convective activity is dominated by the maritime signal. The inclusion of R thus accounts for a large part of the reduction in convective activity in HadAM3 and associated decreases in precipitation and increases in moisture and layer cloud in the middle troposphere (noted in section 4.4). These changes are in turn consistent with the decreased latent heat release, which balances decreased atmospheric radiative cooling.

5.4 Dynamical fields

The changes in dynamical fields are dominated by changes due to convective momentum transport, which are discussed in detail in section 6. In terms of pmsl, R contributes to the increase in the pressure at the winter pole and the decrease at the summer pole. It also contributes to the improvements in the pressure and pressure gradients in northern mid-latitudes. This is a region of large variability and the effects of R are small. However, the improvements are a robust feature found in early versions of R and the latest version. They probably arise through improvements in the representation of planetary-scale waves. The Hadley circulation alters slightly, consistent with the changes in convective activity over land and sea. The upper branch of the Hadley circulation shifts downwards, southwards and increases slightly on the inclusion of R.

6 Impact of convective momentum transport and other parametrization changes.

Again we make use of additional model runs to assess the impact of parametrization changes in the model:
1. HadAM3-R is compared with HadAM2b to give the combined impact of all changes except R.
2. Spin-up runs of HadAM3 and HadAM3-CMT (a run of HadAM3 without convective momentum transport) are used to identify the change in zonal-mean wind acceleration from the individual parametrization schemes and the dynamics scheme.
3. A series of AMIP integrations run during the development of HadAM3 which test the various parametrization changes individually.

6.1 Convective momentum transport

The biggest change in HadAM3 other than the new radiation scheme is the inclusion of convective momentum transport (CMT). As well as directly changing the winds, particularly in the tropics, it also affects a range of other fields through changes in the circulation.

6.1.1Winds

Differences in the winds between HadAM2b and HadAM3 (Figs. 3 and 4) are dominated by the impact of CMT (see Fig. 19 of Gregory et al., 1997). Fig. 20 shows the main impacts of including CMT on zonal-mean wind accelerations by different model schemes, during the first 10 days of the simulation. The direct effect of CMT shows up in the change in convective + boundary layer acceleration (these are combined because they are so strongly coupled and in the boundary layer changes in acceleration in one tend to be compensated by changes in the other). The indirect effects of CMT show up in the change in dynamical acceleration.

The main direct effects (Figs. 20(b) and (d)) are:
1. Weakening of the upper level easterly flow in the ITCZ.
2. Weakening of the westerly flow in the subtropics and middle latitudes.
3. Strengthening of the upper branch of the Hadley circulation (Eta=0.3-0.2) with weakening above and below.

These agree with the findings of Gregory et al. (1997)

Comparing Fig. 20 with Figs. 3 and 4 shows that the only regions where these direct effects dominate are in the upper level ITCZ and at mid latitudes (roughly 30° to 50° N and 30° to 50° S). Dynamical (i.e. indirect) effects sometimes strengthen the response, sometimes change its sign, and sometimes shift its position. The large impact of CMT on the zonal wind (Fig. 20(b)) around Eta = 0.25 in the tropics is offset by the dynamics acceleration (Fig. 20(a)). There is additional dynamical strengthening of the Hadley circulation (Fig. 20(c)), probably arising as a response of the meridional circulation to the forcing of zonal momentum by convection via the Coriolis force (Gregory et al. following Zhang and McFarlane, 1995, and Helfand, 1979).

Other indirect effects mainly arise through transport. In order to illustrate this we show the

mass stream function for the Transformed Eulerian Mean (TEM) circulation in Fig. 21. As with a standard stream function, the gradient represents the strength of the TEM circulation. However, unlike the standard stream function mass is transported along the streamlines. In the absence of diabatic effects the TEM streamlines would be parallel to isentropic surfaces (also shown in the figure). The main difference between the TEM and standard stream functions (compare Figs. 21 and 4) is that there is no Ferrel cell in the former, since this involves reversible changes and no net transport of mass. The effects of transport on the wind tendencies are:

1. In the tropics, to spread the westerly acceleration from the ITCZ (which effectively decreased the easterlies) polewards and down following the Hadley circulation, leading to acceleration of the westerlies on the equatorward side of the subtropical jet, at around 20 N in Fig. 3. This is confirmed by the increased westerly dynamics acceleration in this region.
2. Close to the equator, to shift the acceleration and deceleration patterns in the meridional wind upward in the ascending part of the Hadley circulation. There is a corresponding dipole in the dynamics meridional wind acceleration, which more than balances the opposing convective acceleration tendencies.

6.1.2 Divergence and convection

The increased convergence and divergence when CMT is added are related to increases in the strengths of the Hadley and Walker circulations. There is a potential feedback of CMT on convection via the boundary layer scheme, which could contribute to these changes. CMT increases surface winds by mixing strong winds near the top of the boundary layer with weaker winds near the surface. Changes in the boundary layer accelerations tend to compensate for these changes but the CMT impacts dominate - notice the increased acceleration of the westerlies near the surface between 30 and 60 deg in both hemispheres in Fig. 20(b). The increased winds strengthen the surface fluxes making convection stronger when it occurs. CMT is a major contributor to the increases in precipitation seen in the ITCZ over the continents in Fig. 11 and the decreases to the north. The corresponding decreases in OLR give better agreement with the ERBE climatology (Fig. 13). Improvements in all these fields are particularly striking over Indonesia and the surrounding area.

6.1.3 PMSL

CMT makes the largest contribution to the improvements in local biases in pmsl in northern mid latitudes (Fig. 1). The impact of CMT on pmsl is shown in Fig. 22. It reduces the low pressure bias in the N Atlantic and the pressure gradient error associated with the north-easterly bias in the low level winds south-east of Greenland. However, it increases the easterly bias over northern Eurasia. It also makes a significant contribution to the increased high pressure bias at southern middle latitudes and the decreased westerly bias at around 60° S. The direct effect of CMT on zonal winds (see the zonal wind acceleration in Fig. 20(b)) at mid latitudes is to increase surface westerly winds not to decrease them. The changes in low level winds near 60° N and S must therefore be an indirect effect of CMT, either a local feedback in the dynamics or more indirectly due to large-scale changes in the circulation associated with the direct effect of CMT on the tropical circulation.

6.1.4 Energy and moisture budget

CMT alters the local energy balance and surface heat fluxes. Fig. 23 summarises the impact of non-R changes on the downward surface fluxes. None of the impacts are as large as the impact of R on the latent heat flux (Fig. 19). The biggest changes in Fig. 23 are in the equatorial region. Broadly, there is more latent heat flux out of the ocean (i.e. negative bars on the figure) and less solar radiation reaching the surface in HadAM3-R than in HadAM2b. The larger negative latent heat flux is due to CMT in the eastern equatorial oceans and due to the other non-R changes in the west and central Pacific. CMT redistributes low level winds affecting surface fluxes, boundary layer processes and convective processes. This in turn affects the shortwave radiation reaching the surface via changes in the cloud distribution. Despite the local impacts of CMT, in the global mean it has little impact on the energy budget. The non-R impacts in table 2 arise mainly from changes to the critical relative humidity.

The mean surface parameters used in the various bar charts throughout this paper provide a useful summary of some of the main changes in the model fields. However, as with all the mean

fields used, they should be used with caution. For example, local fluxes in the NW Pacific and NW Atlantic, and in particular the latent heat flux, are very sensitive to small changes in the position of the storm track. However, the regions we have averaged over encompass these small changes and so the local sensitivities can be lost in the mean. This becomes more important in the coupled model because slight shifts in the storm track are amplified when the ocean and atmosphere are allowed to evolve freely.

6.2 MOSES

A detailed study of the impact of the new land surface scheme, MOSES, is given in Cox et al. (1999). The main improvements are in surface fields. The inclusion of soil water phase changes acts to warm the high northern latitudes in winter and autumn. In Fig. 15 this is offset by other changes in parametrizations, the main one being the boundary-layer changes. Increased soil water availability (primarily as a result of increased rootdepths) prevents a spurious drying and warming in the mid-latitudes during summer. Cox et al. also demonstrate that the sensitivity of the model to doubling atmospheric CO_2 is enhanced with the new scheme, because of the inclusion of the dependence of stomatal resistance on CO_2.

6.3 Critical relative humidity (RH_{crit})

As pointed out in section 2, RH_{crit} has been reduced in HadAM3, reducing the amount of layer cloud in the upper troposphere at all latitudes and in the middle troposphere in the extra-tropics. It also leads to small increases in cloud near the top of the boundary layer, particularly in the tropics. These changes are associated with reduced rainfall in the tropics over land improving the model climatology (the non-R changes in Fig. 12 are dominated by the change in RH_{crit}).

The RH_{crit} change is the main non-R contributor to the changes in TOA radiation in table 1. The changes in the cloud distribution are consistent with the decrease in LW cloud forcing (which is more sensitive to upper level cloud) and the increase in SW cloud forcing (which is more sensitive to low level cloud). Both these effects contribute to a decrease in the net downward radiation at TOA and at the surface. The new value of RH_{crit} was chosen so that the decreases in net radiation nearly balance the increases when R is included in the model.

As might be expected from the global calculations in table 1 the RH_{crit} change is the main contributor to the changes in the local shortwave fluxes at the ocean surface (Fig. 23). The solar heating reaching the surface is decreased right across the tropics due to the increased cloud water in the lower troposphere. The overall changes in the ocean surface heat fluxes are dominated by the impact of R on the latent heat flux in the extra-tropics, and by the impact of changing RH_{crit} on the solar heat flux in the tropics.

6.4 Boundary layer

The changes in the boundary layer scheme are relatively minor and are only discussed briefly. However, turning off the rapid mixing in the boundary layer affects the balance between the boundary layer and convection schemes. Essentially the convection scheme does more boundary layer mixing if the boundary layer scheme does not do it. Evidence for this is that the impacts of turning off rapid mixing and turning on CMT are similar in pattern, suggesting that the former enhances the latter. This change in the way the convection scheme operates when rapid mixing is switched off may be the reason for the raising of the convective cloud base in the tropics when the boundary layer changes are made (notice the decrease in convective cloud amount at level 3 in Fig. 9). This effectively reduces the amount of low level cloud, allowing increased solar radiation to reach the surface, which partly offsets the decreased surface solar radiative flux (Fig. 23) associated with the change in RH_{crit}.

The change in mixing length increases friction at the surface. For a given pmsl gradient, the net effect is an increased surface
stress; this reduces near-surface wind speeds and weakens the pmsl gradient. The corresponding

changes in wind tend to compensate for the direct changes in the boundary layer scheme so that the wind stress does not change much. The most obvious impact of these changes is around Antarctica. The boundary layer changes contribute to reducing low-pressure bias over Antarctica (Fig. 1) and to reducing the westerly bias to the north. They also decrease the low-pressure bias in the N Atlantic and the north-easterly bias in the winds between Iceland and Greenland. The boundary layer changes also contribute to the surface temperature changes in HadAM3. Over N. America they are the dominant contribution to the decreases in temperature shown in Fig. 14.

7 Discussion and Conclusions

We have demonstrated that the mean climate of HadAM3 is a significant improvement over HADAM2b and that in most respects it now represents well the observed mean climate during the AMIP period. It compares favourably with other climate models, as shown in the following brief summary comparing basic model fields with those from the ensemble used in AMIP (Gates et al., 1999). The errors in the mean of the AMIP ensemble of models are smaller than the errors in most individual model, so this is a stringent test of the relative performance of a model. For more details of the performance of some of the models used in AMIP and their more recent versions see relevant papers, such as Hurrel et al. (1998), Hack et al. (1998) and Kiehl et al. (1998) for the NCAR model CCM3; McFarlane et al (1992) for the Canadian Climate Centre second generation model (CCC2); Colman and McAvaney (1995) for the Australian Bureau of Meteorology; and Chen and Roeckner (1996) for the MPI model ECHAM4.

Both HadAM2b and HadAM3 have a large high pressure bias in mean sea level pressure over the winter pole. The error is up to 10hPa comparing unfavourably with the AMIP ensemble mean error of up to 4hPa (compare Fig. 1 with Gates et al., Fig. 1). However, the small high pressure bias in other models is often at the expense of errors elsewhere. For example, the ensemble standard deviation is more than 6 hPa over most of the NE Atlantic and N Europe and the errors in HadAM3 are no more than 2 hPa. In the Hadley Centre model the zonal mean zonal winds in the extratropics are considerably better than those of the ensemble mean of AMIP models (compare Fig. 3 with Gates et al. Fig. 6). With the improvements in winds at all latitudes, but particularly in the tropics, HadAM3 performs better than the AMIP ensemble mean throughout the troposphere.

Most climate models are too cold at lower levels in the tropics and in the upper troposphere and lower stratosphere in higher latitudes, and too warm in the tropical lower stratosphere (IPCC, 1995). HadAM2b suffers from most of these errors although the tropical cold bias is worst in the upper troposphere and there is a warm bias in the winter above 200 hPa. The temperature biases are substantially reduced in HadAM3.

Both versions of the Hadley Centre model produce very good simulations of precipitation. HadAM2b has similar errors to the AMIP ensemble mean (Gates et al., Fig. 3) and HadAM3 has somewhat smaller errors. A particular problem area for many models is in representing the precipitation and circulation over the Indonesian region. This has improved considerably in HadAM3, as was shown in the analysis of precipitation, velocity potential and outgoing longwave radiation. The treatment of radiation in HadAM3 is physically much more realistic than in previous general circulation models. Also, the individual radiative terms agree well with observations in the global mean (see table 2). Although there is some tuning in HadAM3 to avoid model drift in the coupled version of the model, the individual radiative terms are not tuned independently. Hence, HadAM3 is producing reasonable numbers (to within estimates obtained from observations) for physically sensible reasons.

We have identified the major improvements in the model's climate with the main changes in model parametrizations that have gone into HadAM3. Each of these improvements is outlined below and is identified with the main parametrization change (or changes) that has impacted on the particular field. Relevant figures are also listed for reference. The main remaining systematic errors are also outlined.

7.1 Main Improvements

(a) The local mean sea level pressure biases are improved - Convective Momentum Transport (CMT) and boundary layer changes, Figs. 1 and 22, section 6.1.3.
(b) Tropical winds are improved - CMT, Figs. 3 and 20, section 6.1.1.
(c) The tropospheric cold bias is reduced - New Radiation scheme (R), Figs. 6, 17 and 18, section 5.1.
(d) The moist bias is reduced - R, RH_{crit}, Fig. 7 and 8, sections 5.3 and 6.3.
(e) The dry bias in the tropical middle troposphere is reduced - R, Fig. 7, section 5.3.
(f) The rainfall and circulation in the Indonesian warm pool is improved - R and CMT, Fig. 5, 11 and 13, sections 5.3 and 6.1.4.
(g) Blocking in the N Pacific is improved significantly - R and CMT, Fig. 2, section 4.1.
(h) Surface and subsurface winter continental temperatures are improved -MOSES, Figs. 14 and 15, section 6.2.
(i) The surface heat fluxes (and sea surface temperature biases in the coupled model) are improved everywhere - R, Figs. 16, 19 and 23, sections 5.3 and 6.1.4. This is the most significant improvement as far as the coupled model is concerned.

7.2 Remaining errors

(a) High pressure bias over the poles - Fig. 1.
(b) Cold bias around the tropopause at high latitudes in summer and in the storm tracks - Fig. 6.
(c) Moist bias in the upper troposphere and related biases in the cloud distribution and optical properties - Fig. 7, 8 and 10.
(d) The Hadley and Walker circulations are too strong - Figs. 4, 5 and 21.
(e) For the coupled model the most significant errors are the excessive cooling of the ocean in the north Pacific and excessive warming in the southern ocean and eastern tropical oceans - Fig. 16.

Current research in the Met. Office and elsewhere is focussing on reducing these model errors. Improvements in vertical advection in the tropopause region reduce the temperature and moisture biases. Increasing the vertical resolution around the tropopause is one way of achieving this. Recent tests with 30 levels in HadAM3 have produced significant improvements in temperature and moisture in the upper troposphere and lower stratosphere. Another way is to use a more accurate advection scheme. Semi-Lagrangian advection has been shown to make similar or greater improvements in other models (Chen and Bates, 1996, and Williamson et al., 1998). With regard to the errors that particularly affect the coupled model, recent tests with improved cloud parametrization in HadAM3 have significantly reduced the cooling of the N Pacific.

Overall, HadAM3 produces a good simulation of current climate when forced with observed sea surface temperatures. In coupled mode (Gordon et al., 1999) it is able to run without flux adjustments, a significant advance on the previous generation of coupled models.

Acknowledgements The authors would like to thank John Edwards for providing the radiation double call tests and Simon Wilson for helping to produce the diagnostics. They would also like to thank Chris Gordon, Alan Grant, Roy Kershaw, Gill Martin, Cath Senior, Tony Slingo, Rod Smith, and Stuart Webster for useful discussions and comments. They would also like to thank Ron Stouffer and an anonymous reviewer for comments on the original draft of the paper.

References

Barkstrom B, Harrison E, Smith G, Green R, Kibler J, Cess R, 1989, Earth Radiation Budget Experiment (ERBE) archival and April 1985 results. Bull Am Meteorol Soc, 70, 1254-1262.

Boer G J, Arpe K, Blackburn M, Deque M, Gates W L, Hart T L, Le Treut H, Roeckner E, Sheinin D A, Simmonds I, Smith R N B, Tokioka T, Wetherald R T and Williamson D, 1992, Some results from an intercomparison of the climates simulated by 14 atmospheric general circulation models. J

Geophys Res, 97, D12, 12771-12786.

Chen M and Bates J R, 1996, A comparison of climate simulations from a semi-Lagrangian and an Eulerian GCM. J Clim, 1126-1149.

Chen C -T and Roeckner E, 1996, A comparison of Satellite Observations and Model Simulations of Column-Integrated Moisture and Upper-Tropospheric Humidity. J Clim, 1561-1585.

Clough S A, F X Kneizys and R W Davies, 1989, Line Shape and the Water Vapour Continuum. Atmos. Res., 23, 229-241.

Colman R A and McAvaney B J, 1995, Sensitivity of the climate response of an atmospheric general circulation model to changes in convective parametrization and horizontal resolution. J Geophys Res, 100, D2, 3155-3172.

Cox P.M., Betts R.A., Bunton C.B., Essery R.L.H., Rowntree P.R. and Smith J., 1999. The impact of new land surface physics on the GCM simulation of climate and climate sensitivity. Climate Dynamics, 15, 183-203.

Cullen M, 1993, The Unified forecast/climate model. Meteorol. Mag. 122, 81-94.

Cusack, S., A. Slingo, J. M. Edwards and M. Wild, 1998: The radiative impact of a simple aerosol climatology on the Hadley Centre climate model. Quart. Journal of the Royal Meteor. Soc., 124, pp 2517-2526.

Cusack, S., J. M. Edwards and J. M. Crowther, 1999: Investigating k-distribution methods for parametrizing gaseous absorption in the Hadley Centre climate model. J. Geophys. Res., 104, 2051-2057.

Da Silva A M, Young C C and Levitus S, 1994, Atlas of surface marine data 1994, Volume 1: Algorithms and procedures. NOAA Atlas NESDIS, 6.

Edwards J M , Slingo A, 1996, Studies with a flexible new radiation code. I: choosing a configuration for a large-scale model. Q J R Meteorol Soc, 122, 689-719.

Ferranti L, Molteni F and Palmer T N, 1994: Impact of localised tropical and extratropical SST anomalies in ensembles of seasonal GCM integrations. Q J R Meteorol Soc 124, 1613-1646.

Gates W L, 1992, AMIP: The Atmospheric Model Intercomparison Project. Bull Amer Meteorol Soc, 73, 1962-1970.

Gates W L, Boyle J, Covey C, Dease C, Doutriaux C, Drach R, Fiorino M, Gleckler P, Hnilo, Marlais S, Phillips T, Potter G, Santer B D, Sperber K R, Taylor K and Williams D, 1999, An overview of the results of the Atmospheric Model Intercomparison Project (AMIP). Submitted to Bull Am Met Soc.

Gibson J K, Kallberg P, Uppala S, Hernandez A, Nomura A, Serrano E, 1997, ERA description. ECMWF Re-Analysis Project Series, 1.

Gordon C, Cooper C, Senior C, Banks H, Gregory J, Johns T, Mitchell J and Wood R, 1999, The simulation of SST, sea ice extents and ocean heat transports in a coupled model without flux adjustments. Climate Dynamics, to appear.

Gregory D, 1995, A consistent treatment of the evaporation of rain and snow for use in large-scale models. Mon. Weather Rev., 123, 2716-2732.

Gregory D and Allen S, 1991, The effect of convective scale downdrafts upon NWP and climate simulations. Ninth conference on numerical weather prediction. Denver, Colorado, Amer Met Soc, 122-123.

Gregory D, Kershaw R, Inness P M , 1997, Parametrization of momentum transport by convection. II: Tests in single-column and general circulation models. Q J R Meteorol Soc 123: 1153-1183.

Gregory, D. and Morris, D., 1996: The sensitivity of climate simulations to the specification of mixed phase clouds. Clim Dyn 12, 641-651.

Gregory D and Rowntree P R, 1990, A mass flux convection scheme with representation of cloud ensemble characteristics and stability dependent closure. Mon Weather Rev. 118, 1483-1506.

Gregory D, Shutts G J and Mitchell J R, 1998, A new gravity-wave-drag scheme incorporating anisotropic orography and low-level wave breaking: Impact upon the climate of the UK Meteorological Office Unified Model. Q J R Meteorol Soc 124, 463-494.

Hack J J, Kiehl J T and Hurrell J W, 1998, The hydrologic and thermodynamic characteristics of the NCAR CCM3. J Clim, 11, 1179-1206.

Harrison E F, Minnis P, Barkstrom B R, Ramanathan V, Cess R D, Gibson GG, 1990, Seasonal variation of cloud radiative forcing derived from the Earth Radiation Budget Experiment. J Geophys Res, 95, 18687-18703.

Helfand H M, 1979, The effect of cumulus friction on the simulation of the January Hadley circulation by the GLAS model of the general circulation. J Atmos Sci, 36, 1827-1843.

Hurrell J W, Hack J J, Boville B A, Williamson D L and Kiehl J T, 1998, The dynamical simulation of the NCAR community climate model version 3 (CCM3). J Clim, 11, 1207-1236.

IPCC (intergovernmental Panel on Climate Change), 1995: Climate Change 1995. The science of climate change. J T Houghton, L G Meira Filho, B A Callander, N Harris, A Kattenberg and K Maskell (eds.), Cambridge University Press, Cambridge, U K.

Johns T C, Carnell R E, Crossley J F, Gregory J M, Mitchell J F B, Senior C A, Tett S F B and Wood R A, 1997, The second Hadley Centre coupled ocean-atmosphere GCM: model description, spinup and validation. Clim Dyn, 13, 103-134.

Kallberg P, 1997, Aspects of the re-analysed climate. ECMWF Re-Analysis Project Series, 2.

Kalnay E, Kanamitsu M, Kistler R, Collins W, Deaven D, Derber J, Gandin L, Saha S, White G, Woollen J, Zhu Y, Chelliah M, Ebisuzaki W, Higgins W, Janowiak J, Mo K C, Ropelewski C Wang J, Leetma A, Reynolds R, Jenne R, 1995: The NMC/NCAR 40-year reanalysis project. Bull Amer Met Soc, 77, 437-473.

Keating G M, Young D F and Pitts M C, 1987, Ozone reference models for CIRA. Adv Space Res, 7, 105-115.

Kiehl J T and Trenberth K E, 1997, Earth's annual global mean energy budget. Bull Amer Met Soc, 78, 197-208.

Kiehl J T, Hack J J and Hurrell J W, 1998, The energy budget of the NCAR Community Climate Model: CCM3. J Clim, 11, 1151-1178.

Lean J and Rowntree P R, 1997, Understanding the sensitivity of a GCM simulation of Amazonian deforestation to the specification of vegetation and soil characteristics. J Clim, 10, 1216-1235.

Legates D R and Willmott C J, 1990, Mean seasonal and spatial variability in global surface air temperature. Theoretical and Applied Climatology, 41, 11-21.

Li D, Shine K P, 1995, A 4-Dimensional Ozone Climatology for UGAMP Models. UGAMP Internal Report No 35., April 1995.

Martin G M, and Soman M K, 1999, Effects of changing physical parametrizations on the simulation

of the Asian summer monsoon in the UK Meteorological Office Unified Model. Submitted to Clim Dyn.

McFarlane N A, Boer G J, Blanchet J P and Lazare M, 1992, The Canadian Climate Centre Second-Generation General Circulation Model and its equilibrium climate. J Clim, 5, 1013-1044.

McNally A P and Vesperini M, 1996, Variational analysis of humidity information from TOVS radiances. Q J R Meteorol Soc, 122, 1521-1544.

McPeters R D, Heath, D F and Bhartia P K, 1984, Averaged ozone profiles for 1979 from the Nimbus 7 SBUV instrument. J Geophys Res, 89, 5199-5214.

Roberts R E, J E A Selby and L M Biberman, 1976, Infrared continuum absorption by atmospheric water vapour in the 8 - 12 micron window. Appl. Optics., 15, 2085-2090.

Senior C and Mitchell J F B, 1993, CO_2 and climate: The impact of cloud parametrization. J. Clim. 6: 393-418.

Slingo A, 1989, A GCM parametrization for the shortwave radiation properties of water clouds. J Atmos Sci, 46, 1419-1427.

Slingo A and Wilderspin R, 1986, Development of a revised long-wave radiation scheme for an atmospheric general circulation model. Q J R Meteorol Soc, 112, 371-386.

Smith R N B, 1990, A scheme for predicting layer clouds and their water content in a general circulation model. Q J R Meteorol Soc 116: 435-460.

Smith R N B, 1993, Experience and developments with the layer cloud and boundary layer mixing schemes in the UK Meteorological Office Unified Model. In Proceedings of the ECMWF/GCSS workshop on parametrization of the cloud-topped boundary layer, 8-11 June 1993, ECMWF, Reading, England.

Stratton, R A, 1999, A high resolution AMIP integration using the Hadley Centre model HadAM2b. Clim Dyn, 9-28.

Tibaldi, S and Molteni, F, 1990, On the operational predictability of blocking. Tellus 42A: 343-365.

Warren, S.G., Hahn,C.J., London, J., Chervin, R.M. and Jenne, R.L., 1988: Global distribution of total cloud cover and cloud type amounts over the ocean. NCAR Tech. note.

Williamson D L, Olsen J G and Boville B A, 1998, A comparison of semi-Lagrangian and Eulerian tropical climate simulations. Mon Wea Rev., 126, 991-1000.

Xie P and Arkin P A, 1997, Global precipitation: a 17-year monthly analysis based on gauge observations, satellite estimates, and numerical model outputs. Bull Am Met Soc, 78, 2539-2558.

Zhang G J and McFarlane N A, 1995, Role of convective scale momentum transport in climate simulation. J Geophys Res, 100, 1417-1426.

Figures

Fig. 1 Latitude-longitude maps of mean sea level pressure. Ten year December to February mean from 1979 to 1988 for model and climatological data as follows: (a) HadAM3, (b) HadAM3 - HadAM2b, (c) HadAM2b - ECMWF reanalysis, (d) HadAM3 - ECMWF reanalysis. The units are hPa, the contour interval is 4 hPa in panel (a) and 2 hPa in the other panels. Negative differences are shaded.

Fig. 2 Blocking index (as defined by Tibaldi and Molteni, 1990) as a function of longitude for the northern hemisphere. Ten year mean for December to February.

Fig. 3 As Fig. 1, but latitude-pressure cross section of zonal mean zonal wind. The units are ms^{-1} and the contour interval is $5ms^{-1}$ in panel (a) and $2ms^{-1}$ in the other panels. Easterly winds are shaded.

Fig. 4 As Fig. 3, but meridional wind. The contour interval is $0.5ms^{-1}$ in panel (a) and $0.\ 2ms^{-1}$ in the other panels. Southward winds are shaded.

Fig. 5 As Fig. 1, but velocity potential at 200 hPa (a) HadAM3, (b) HadAM2b and (c) ECMWF reanalysis. The units are $10^6m^2s^{-1}$ and the contour interval is $2x10^6m^2s^{-1}$. Negative values are shaded. Divergent winds point from negative to positive velocity potential.

Fig. 6 As Fig. 3, but zonal mean temperature. The units are K and the contour interval is 10K in panel (a) and 1K in the other panels. Negative values are shaded.

Fig. 7 As Fig. 3, but zonal mean relative humidity. The units are % and the contour interval is 10% in panel (a) and 2% in the other panels. Negative values are shaded.

Fig. 8 Latitude-Eta cross section of zonal mean log(specific humidity) for December to February. (a) HadAM3, (b) HadAM3 - HadAM2b. Fields are on model levels labelled with a value of Eta = average pressure of the level (hPa) x 0.001. The units are log(kg/kg) and the contour interval is 0.2 in panel (a) and 0.02 in panel (b). Negative values are shaded.

Fig. 9 As Fig. 8, but zonal mean convective cloud amount. The units are fractions of a grid box. Differences less than -0.015 are shaded.

Fig. 10 As Fig. 9, but zonal mean layer cloud amount for June to August. Negative differences are shaded.

Fig. 11 As Fig. 1, but precipitation evaluated against the CMAP climatology (Xie and Arkin, 1997). The units are $mmday^{-1}$. The plots use an uneven scale defined in the keys.

Fig. 12 Bar chart for selected latitude bands of annual mean precipitation errors for HadAM2b, HadAM3-R (HadAM3 but with the HadAM2b radiation scheme) and HadAM3 compared with observations from the CMAP climatology. The precipitation is in units of $mmday^{-1}$. The regions are as follows: globe land - all land; globe sea - 56S to 56N (i.e. mainly ice free); tropics - 21S to 21N; N Hem land - 21N to 90N; N Hem sea - 21N - 56N; S Hem land - 59S to 21S; S Hem sea - 56S to 21S.

Fig. 13 As Fig. 1 but Outgoing Longwave Radiation (OLR) at the top of the atmosphere evaluated against the ERBE climatology (Barkstrom et al., 1989). The units are Wm^{-2} and the contour interval is $25Wm^{-2}$ in panel (a) and $10Wm^{-2}$ in the other panels. Negative values are shaded.

Fig. 14 As Fig. 1 but 1.5m temperature evaluated against Legates and Willmott climatology (1990). Difference fields are plotted only over land north of 60°S. The units are K and the shading interval is 5K in panel (a) and 2K in the other panels.

Fig. 15 Bar chart for selected regions of annual mean (unless otherwise stated) 1.5m temperature errors over land evaluated against the Legates and Willmott climatology. Grid points higher than 1500m are excluded. The temperatures are in K. The regions are as follows: global mean; tropics - 21S to 21N; N Hem 21N to 90N; S Hem - 59S to 21S.

Fig. 16 (a) Bar chart for selected regions of annual mean net surface heat fluxes into the ocean in HadAM2b and HadAM3. (b) Map showing the selected regions. The heat fluxes are in Wm^{-2}.

Fig. 17 Latitude-Eta cross sections of the impact of the new radiation scheme on zonal mean temperature. All fields are HadAM3-HadAM3-R. (a) Temperature difference for December to February 10 year mean. The contour interval is 1K. (b) Difference in net heating for 10 day 'spin-up' integrations in December at the start of the AMIP integrations. The contour interval is $0.1Kday^{-1}$ (c) As (b) but the difference in shortwave heating. (d) As (b) but the difference in longwave heating.

Fig. 18 As Fig. 17 but the difference between radiative heating rates from the HadAM3 (R) and

HadAM2b radiation schemes from a 1 month 'double call' test of HadAM2b. The contour interval is $0.1 K day^{-1}$. (a) Shortwave heating, (b) longwave heating, (c) clear-sky shortwave heating, (d) clear-sky longwave heating.

Fig. 19 As Fig. 16 but for differences in the individual surface fluxes between HadAM3 and HadAM3-R. Positive bars indicate an increase in the downward flux and vice versa.

Fig. 20 Latitude-Eta cross sections of the impact of CMT on zonal-mean acceleration. All fields are HadAM3 - HadAM3-CMT from 10 day 'spin-up' integrations in December. The contour interval is 0.5 $ms^{-1}day^{-1}$. (a) Difference in zonal wind acceleration from the dynamics scheme, (b) Difference in zonal wind acceleration from convection and boundary layer schemes combined, (c) as (a) but for meridional wind, (d) as (a) but for meridional wind.

Fig. 21 Latitude-pressure cross section of the transformed Eulerian mean circulation stream function (solid lines) and zonal mean potential temperature (dashed lines) for December to February for HadAM3. The streamfunction units are $10^6 m^2 s^{-1}$, the contour interval is $2x10^6 m^2 s^{-1}$ and negative values are shaded. The units for potential temperature are K and the contour interval is 5K; values greater than 365 K are not shown.

Fig. 22 Latitude-longitude map of the impact of convective momentum transport on mean sea level pressure. December to February seasonal ten year mean. The contour interval is 2hPa and negative values are shaded.

Fig. 23 As Fig. 19 but for HadAM3-R minus HadAM2b.

Fig. 1 PMSL

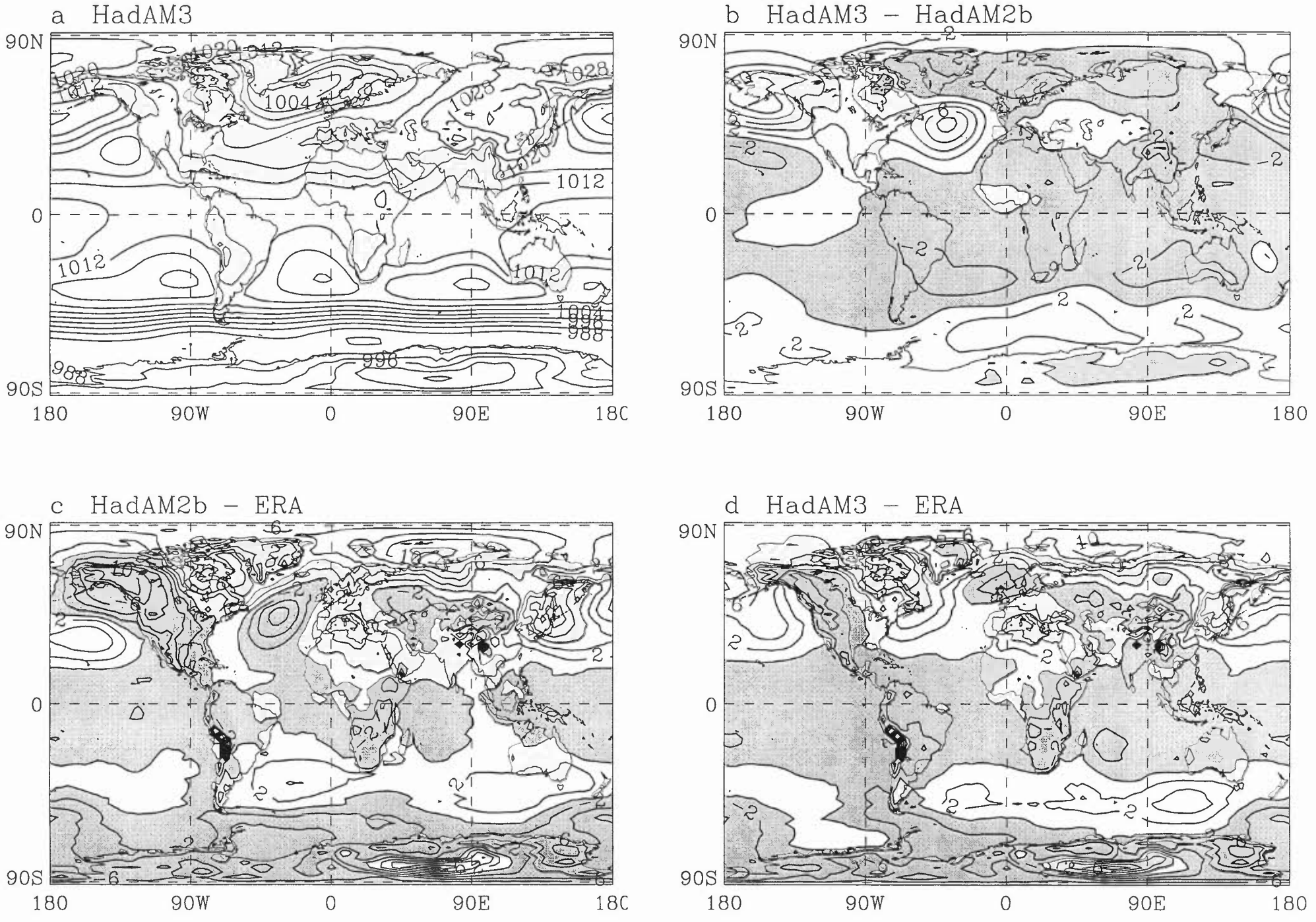
a HadAM3
b HadAM3 – HadAM2b
c HadAM2b – ERA
d HadAM3 – ERA
90N
0
90S
180
90W
0
90E
180
1004
1012
1028
996
988
2
-2
6
-6
10

Fig.2 Blocking index northern hemisphere

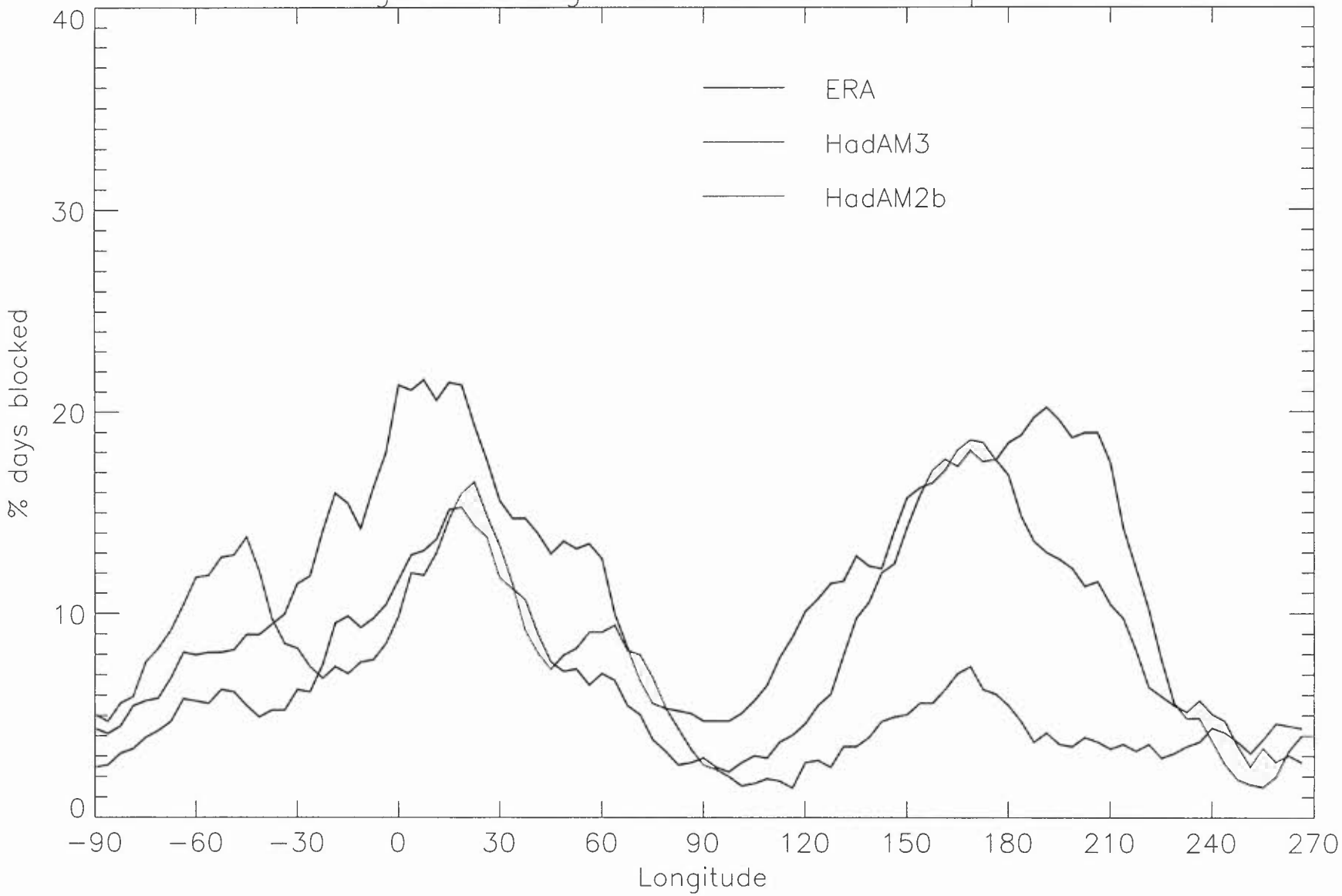

Fig. 3 Zonal mean U wind

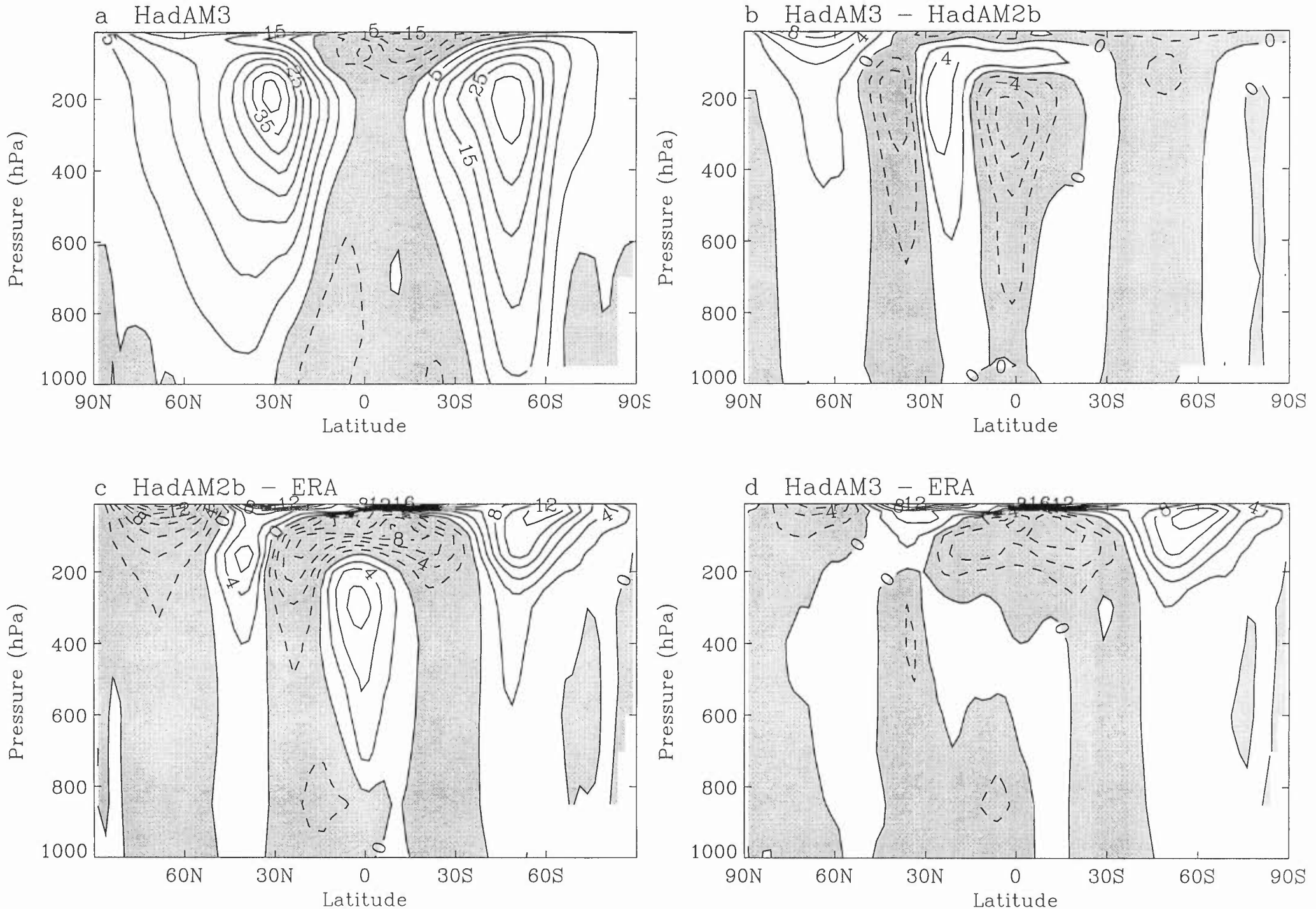

Fig. 4 Zonal mean V wind

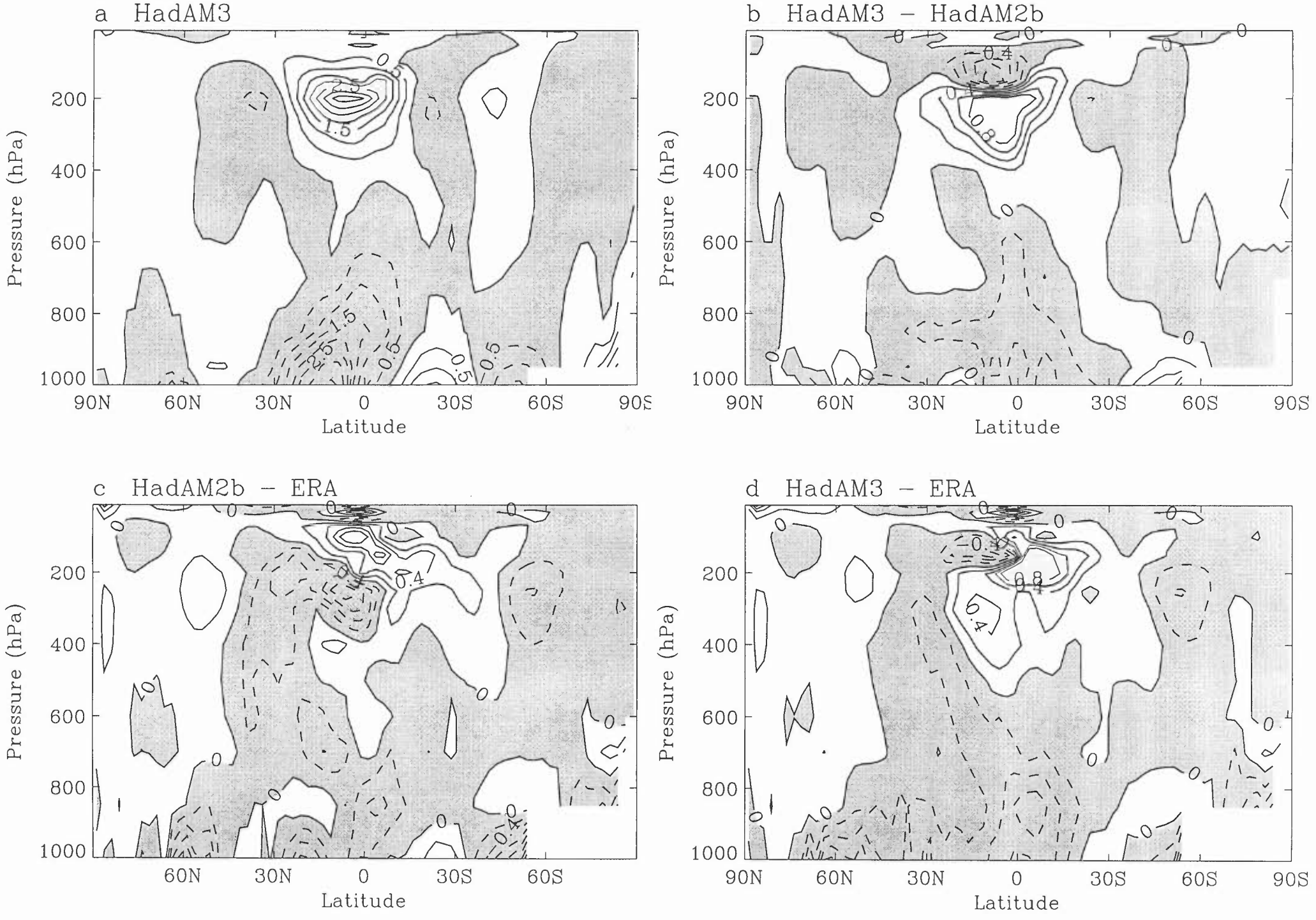

Fig.5 Velocity Potential at 200 hPa

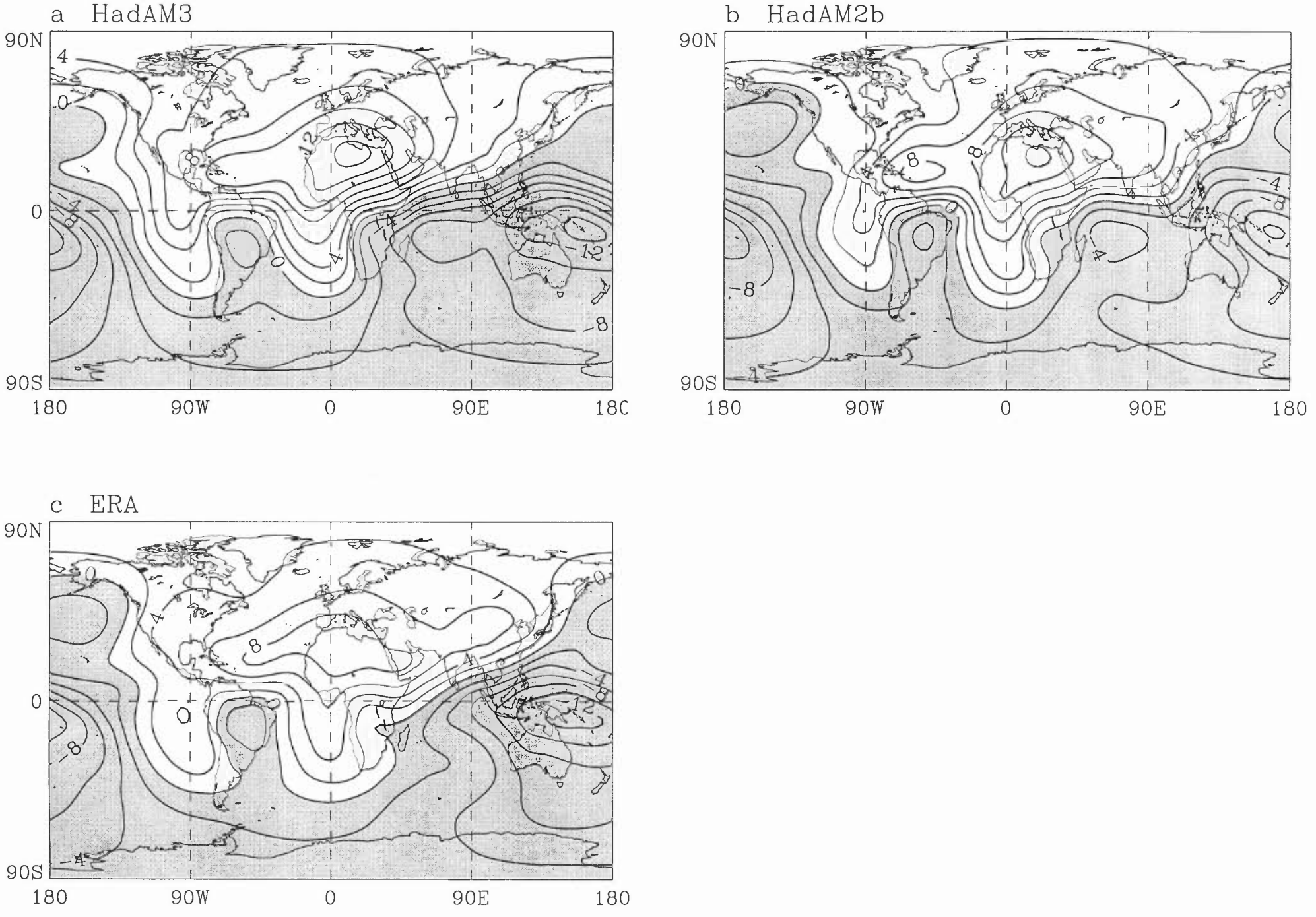

Fig.6 Zonal mean Temperature

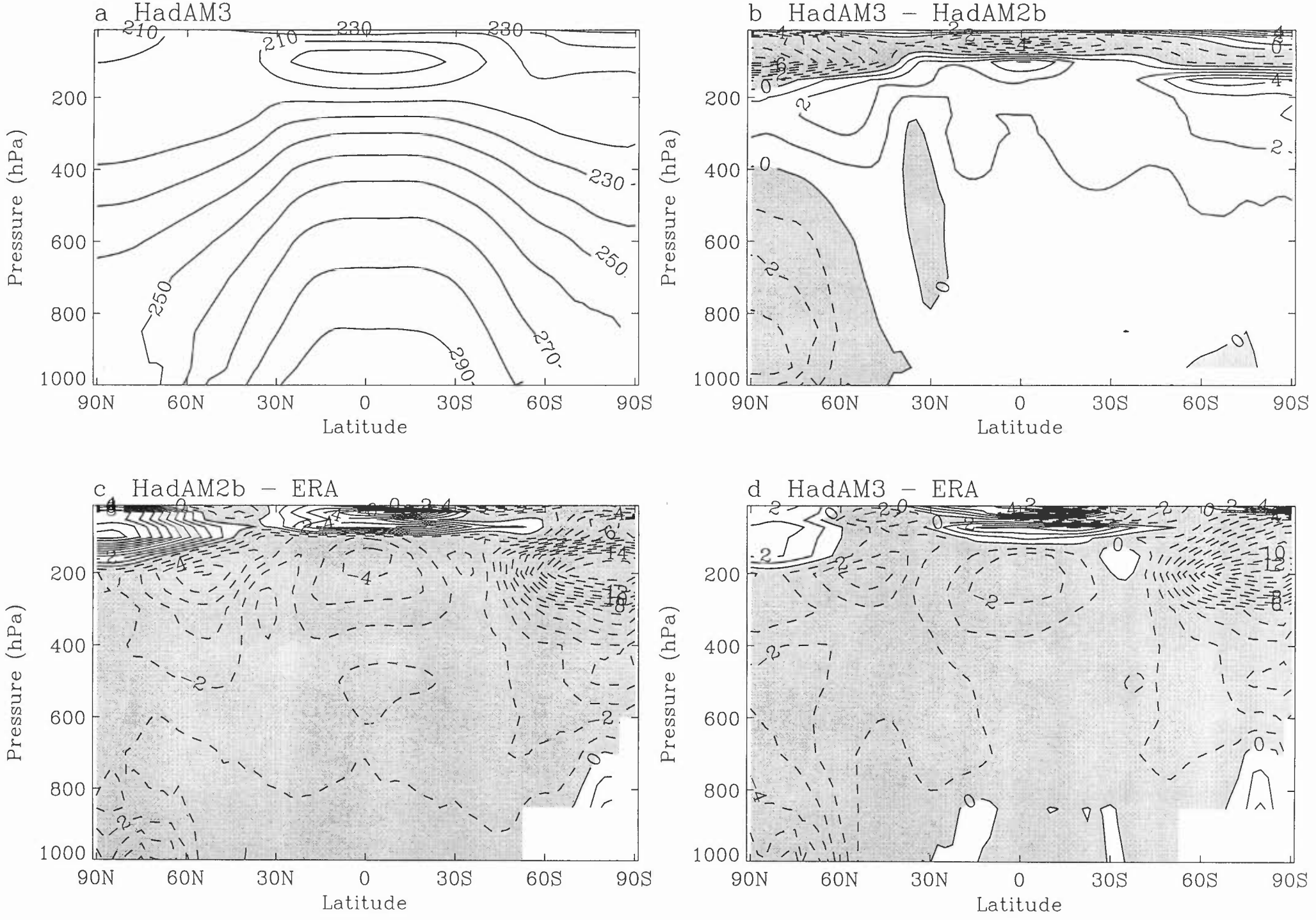

Fig.7 Zonal mean Relative Humidity

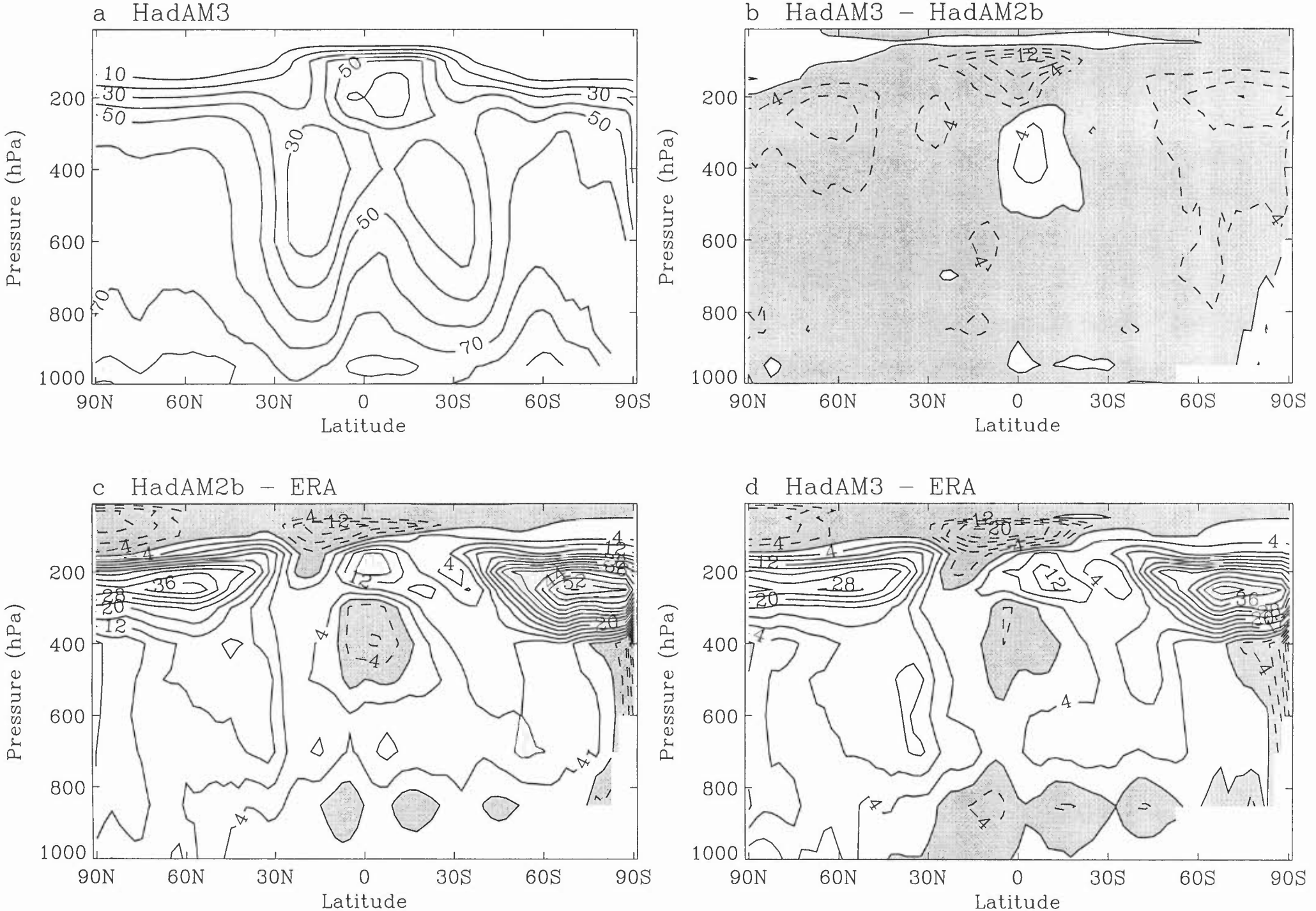

Fig.8 Zonal mean log(Specific Humidity)

a HadAM3

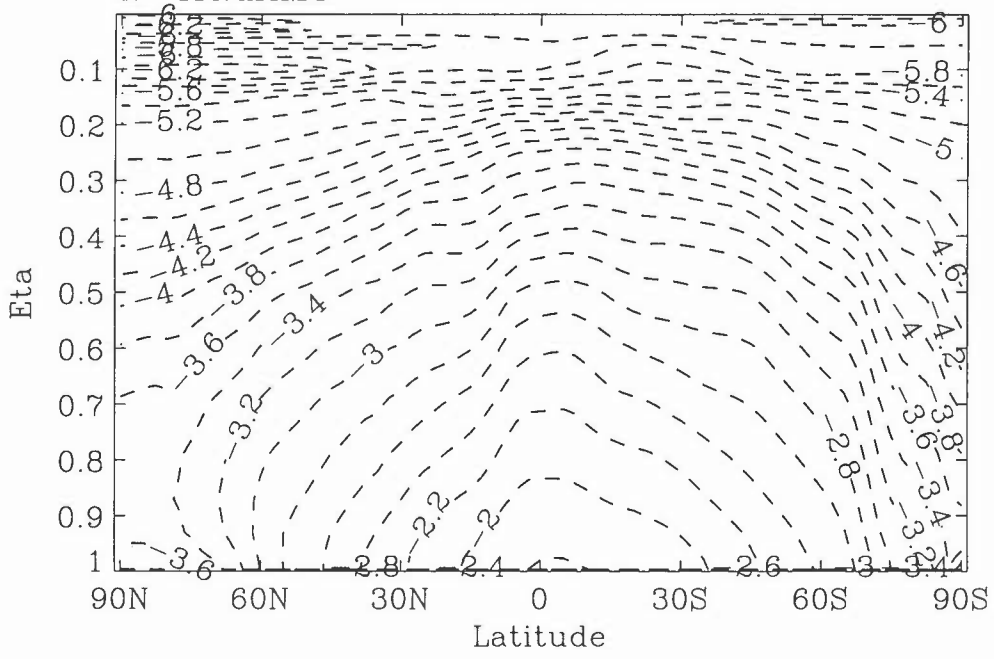

b HadAM3 − HadAM2b

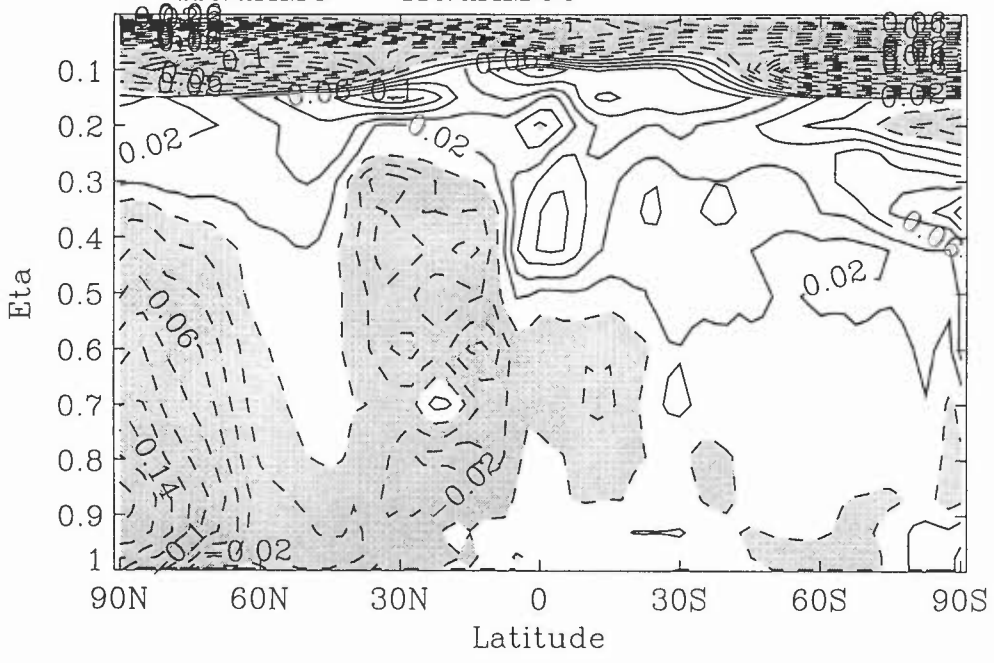

Fig.9 Zonal mean Convective Cloud

a HadAM3

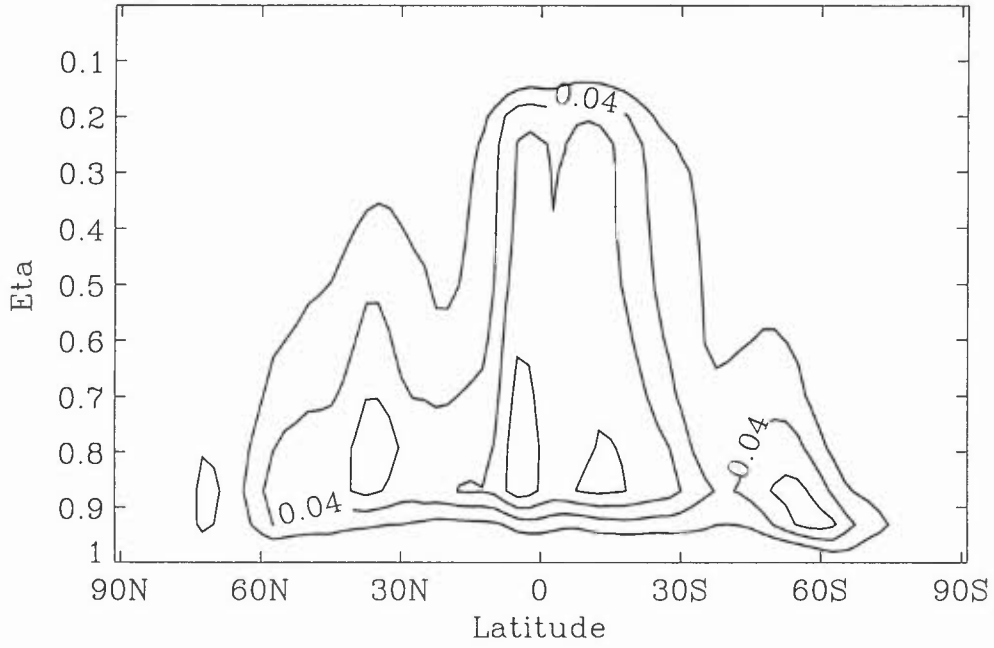

b HadAM3 − HadAM2b

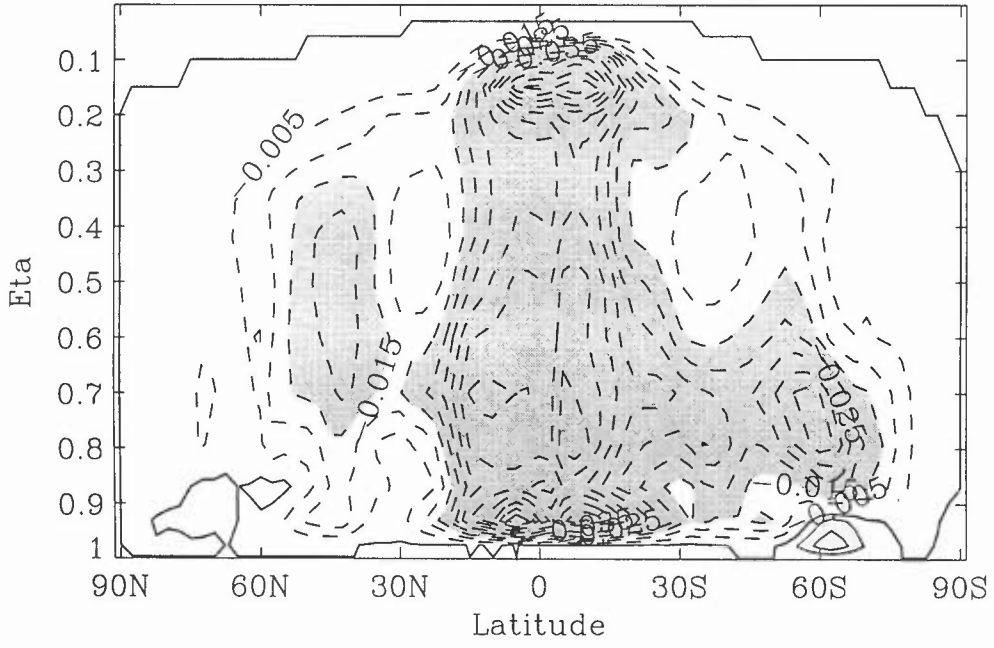

Fig.10 Zonal mean Layer Cloud

a HadAM3

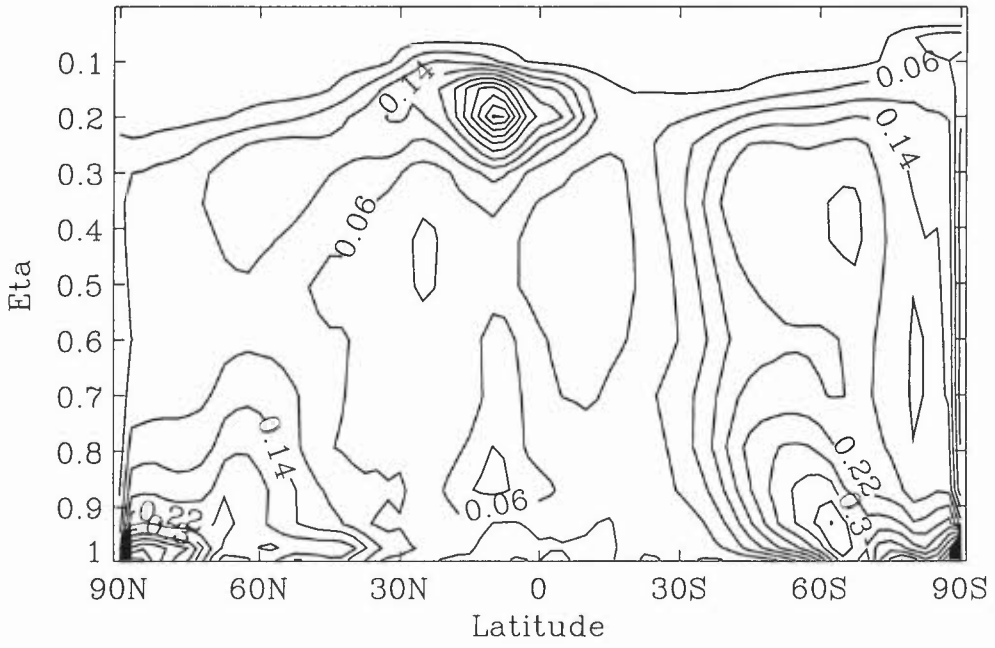

b HadAM3 − HadAM2b

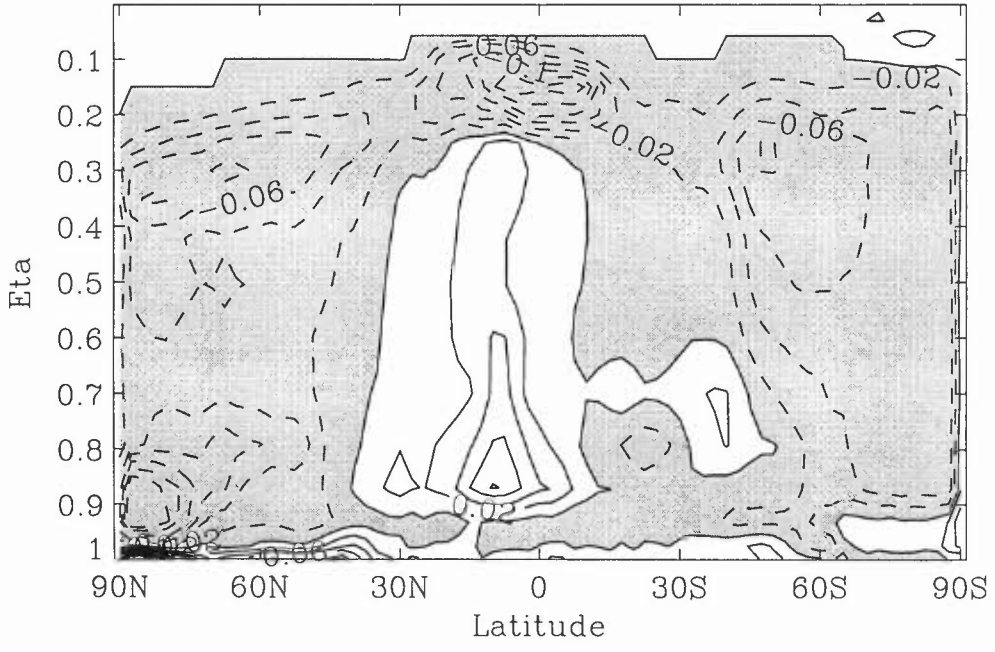

Fig.11 Precipitation

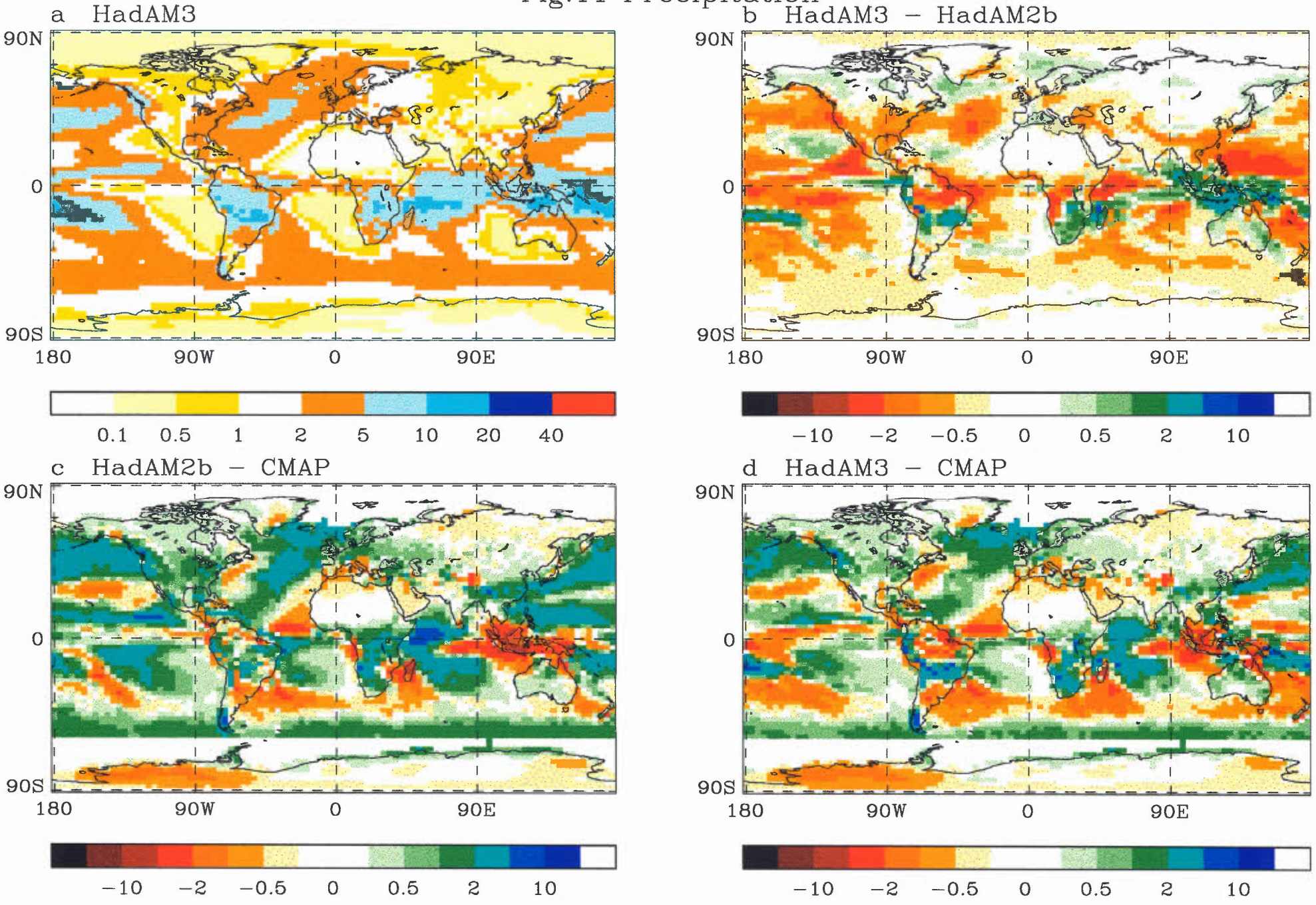

Fig. 12 Precipitation rms errors, compared with CMAP (mm/day)

- globe land - globe
- globe sea - 56 S to 56 N (i.e. mainly ice free)
- tropics - 21 S to 21 N
- N Hem land - 21 N to 90 N
- N Hem sea - 21 N to 56 N
- S Hem land - 59 S to 21 S
- S Hem sea- 56 S to 21 S

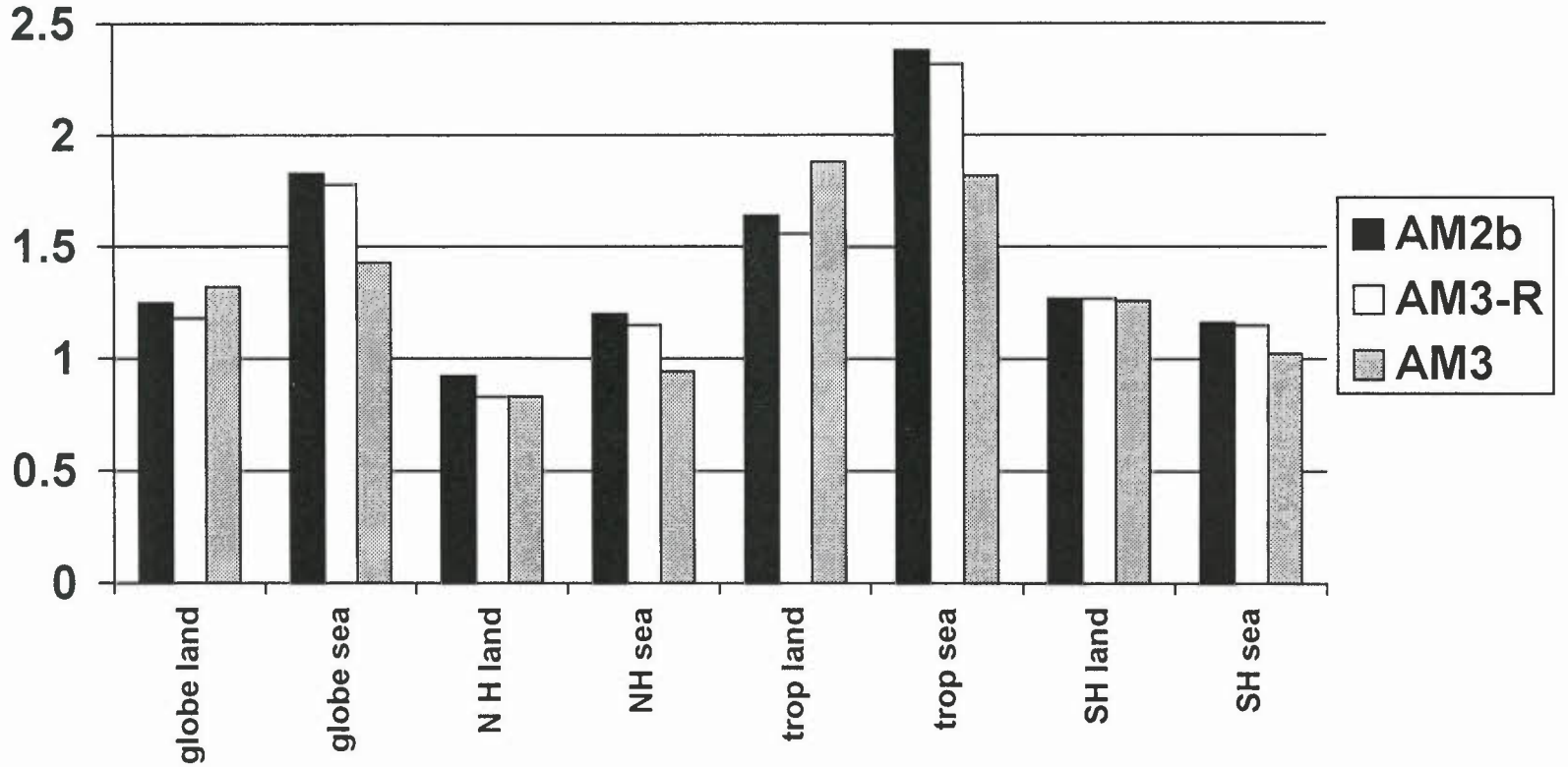

Fig.13 OLR

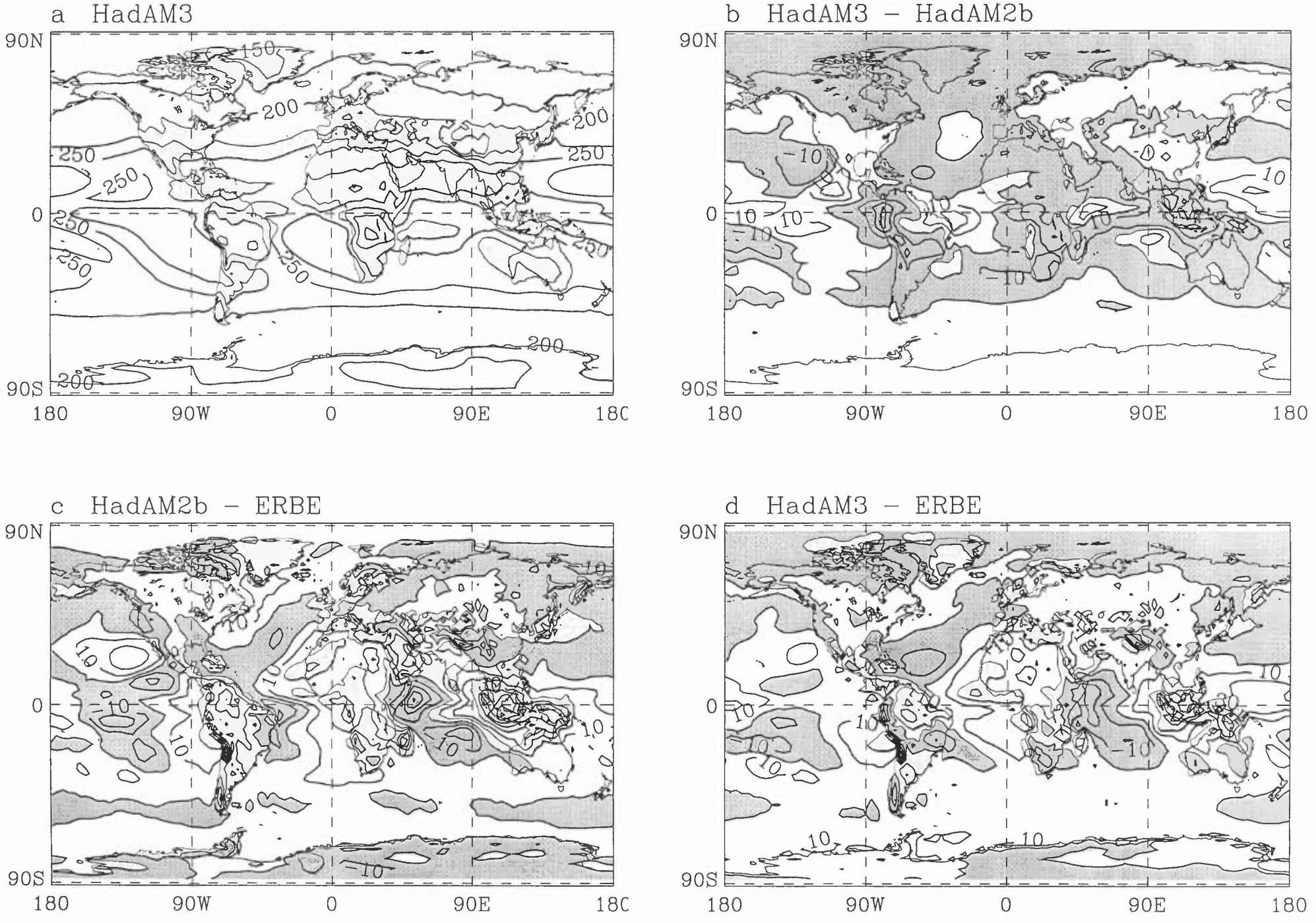
a HadAM3
b HadAM3 − HadAM2b
c HadAM2b − ERBE
d HadAM3 − ERBE
90N
0
90S
180
90W
0
90E
180
150
200
250
−10
10

Fig.14 1.5m temperature

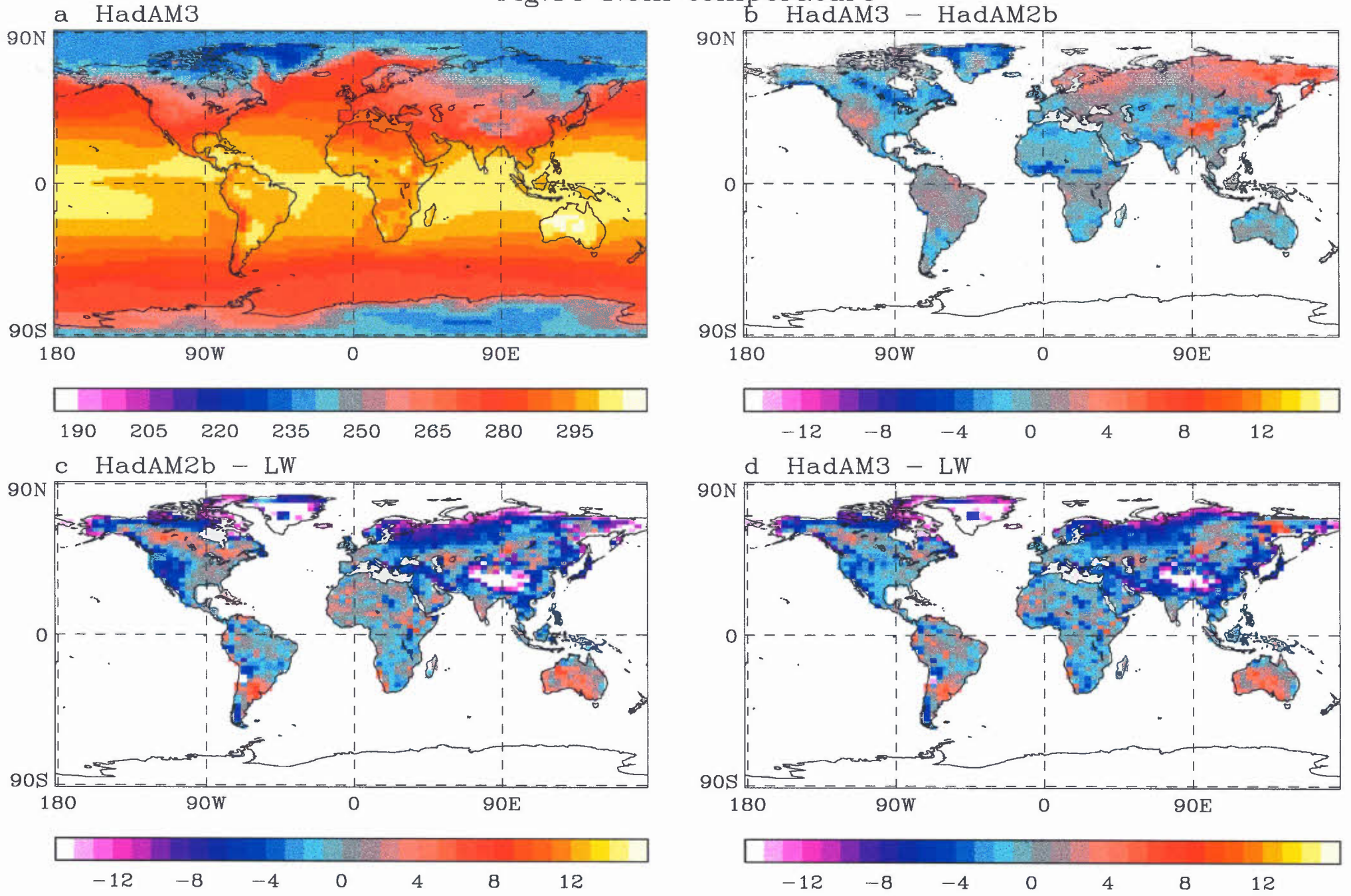

Fig. 15 1.5 m temperature errors

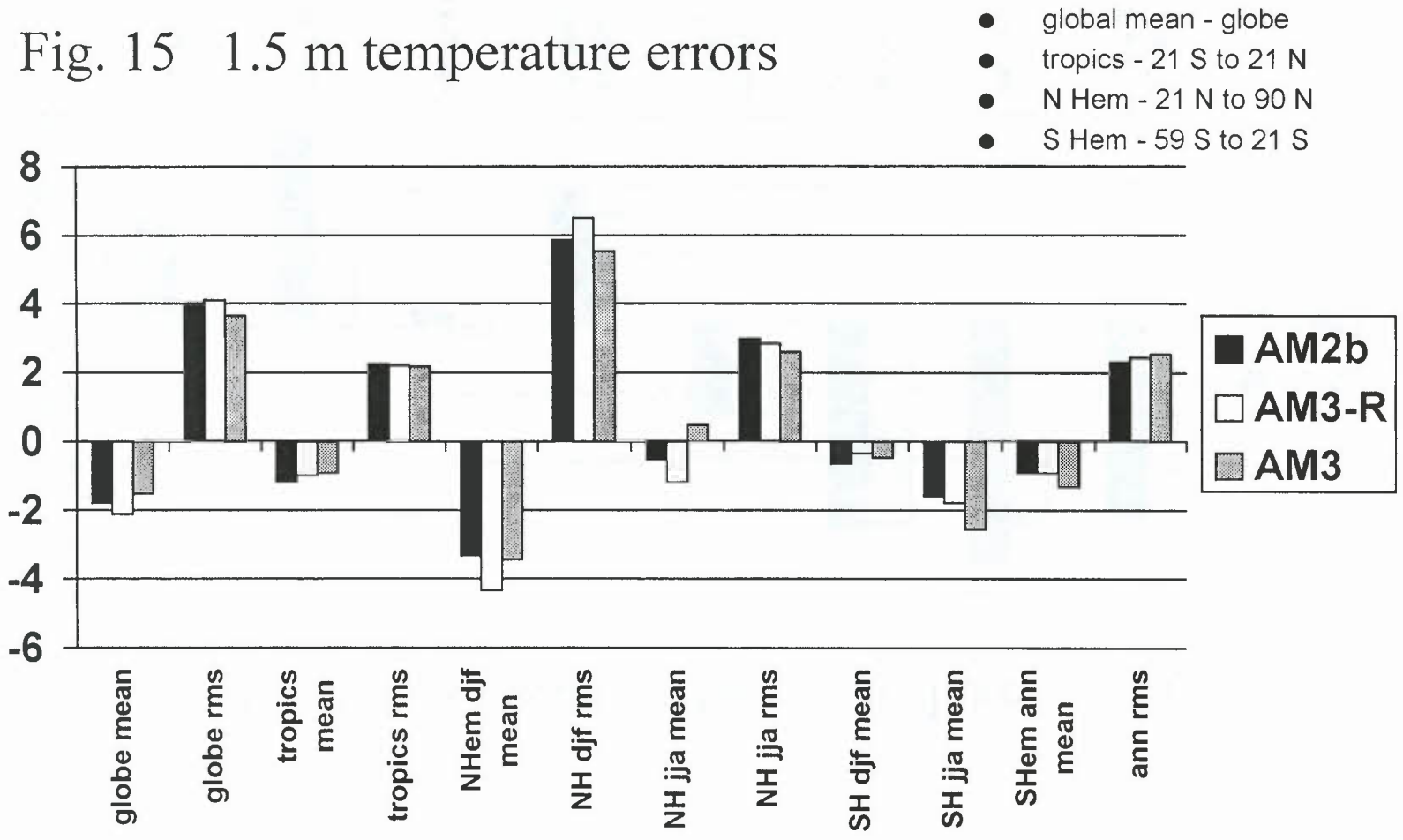

Fig. 16 (a) Net ocean surface heat fluxes (Wm^{-2})

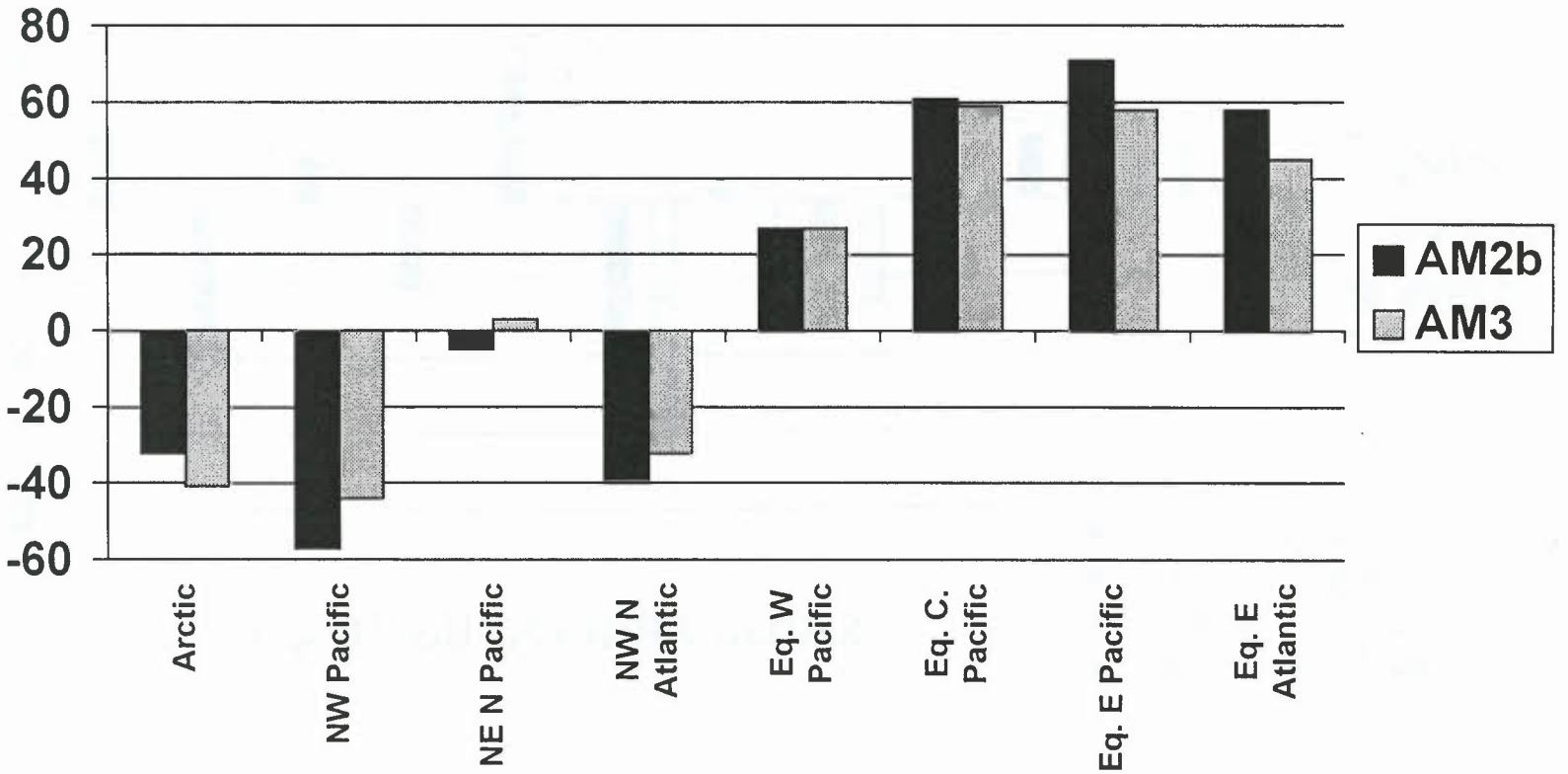

Fig.16(b)

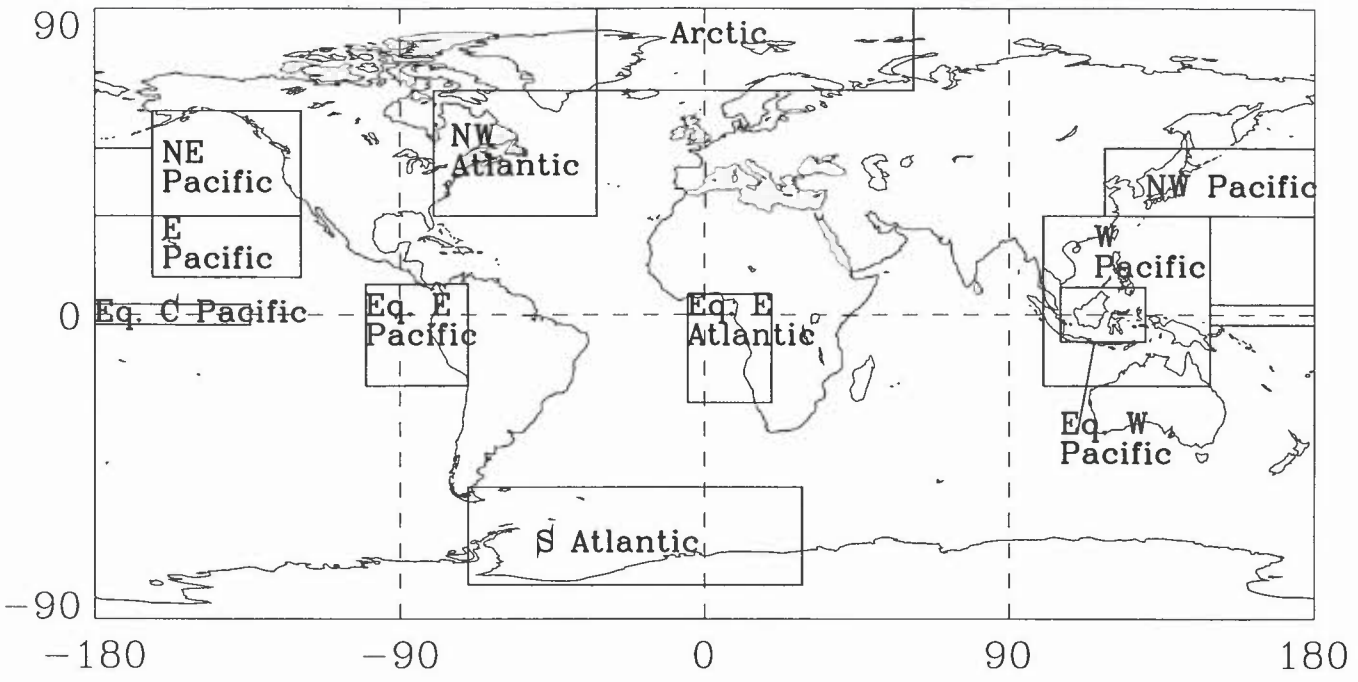
90
0
−90
−180
−90
0
90
180
Arctic
NW Atlantic
NE Pacific
E Pacific
NW Pacific
W Pacific
Eq. C Pacific
Eq. E Pacific
Eq. E Atlantic
Eq. W Pacific
S Atlantic

Fig 17

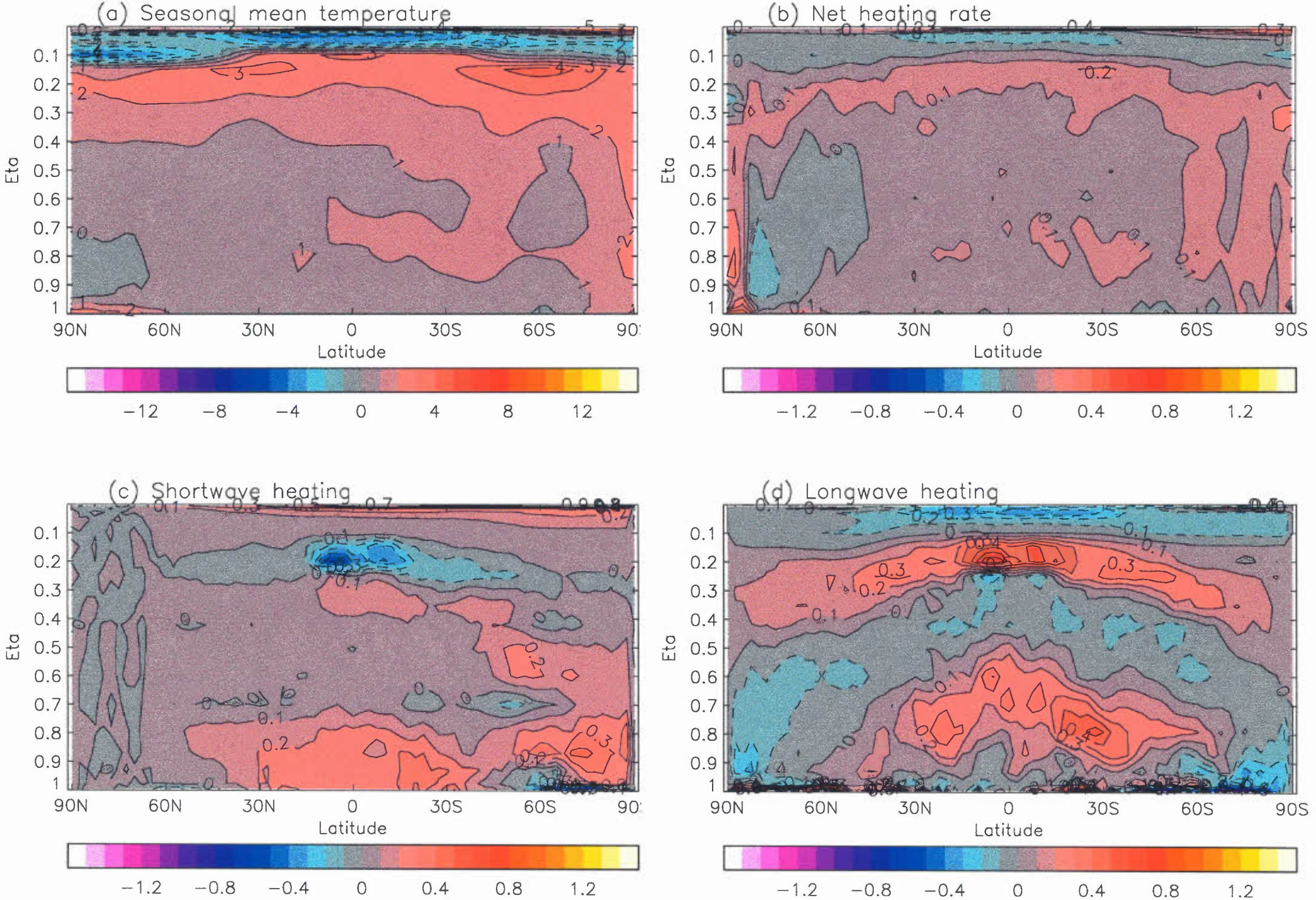
(a) Seasonal mean temperature
(b) Net heating rate
(c) Shortwave heating
(d) Longwave heating
Eta
Latitude
90N
60N
30N
0
30S
60S
90S
−12
−8
−4
0
4
8
12
−1.2
−0.8
−0.4
0.4
0.8
1.2

Fig 18

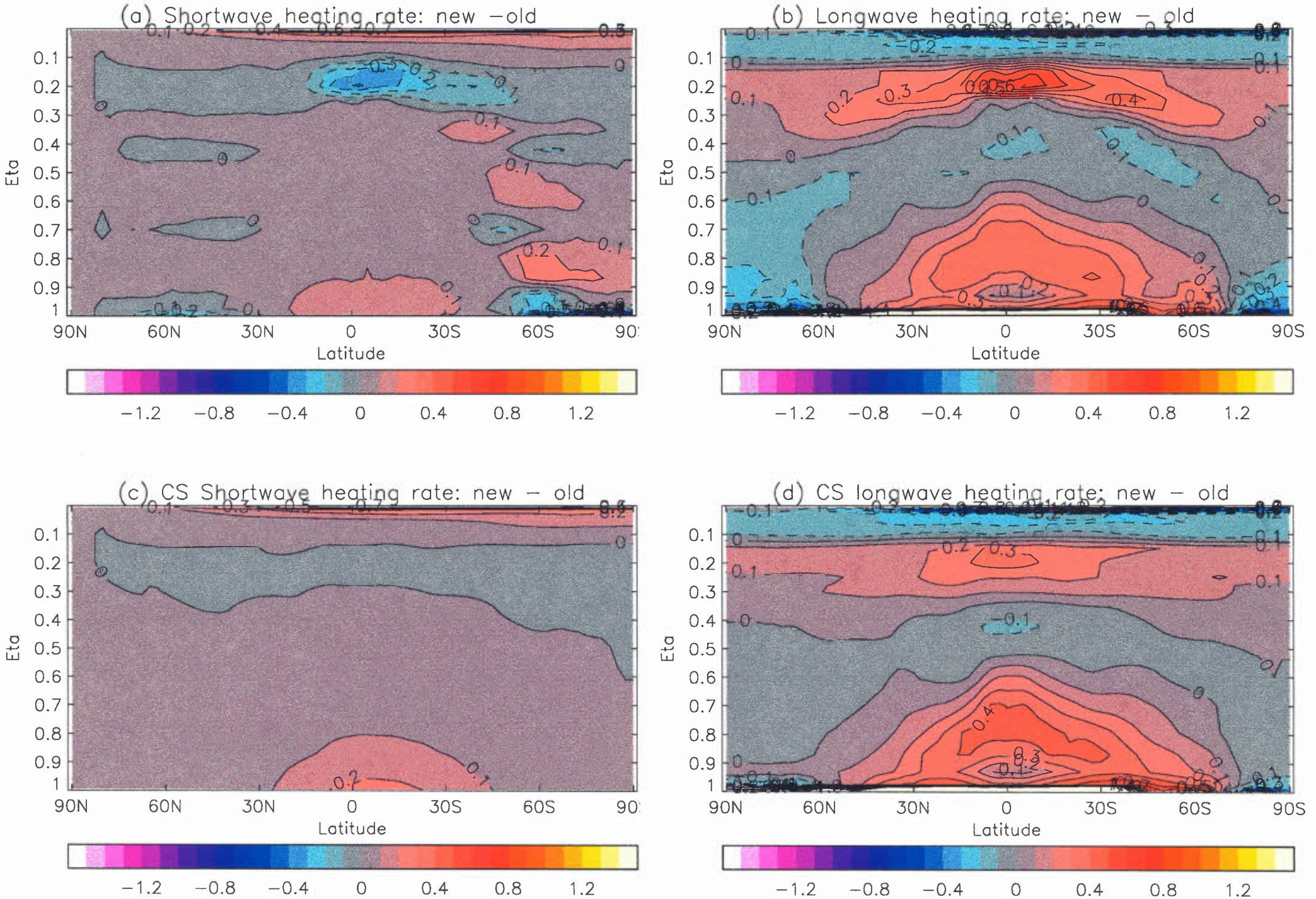
(a) Shortwave heating rate: new −old
(b) Longwave heating rate: new − old
(c) CS Shortwave heating rate: new − old
(d) CS longwave heating rate: new − old
Eta
Latitude
90N
60N
30N
0
30S
60S
90S
−1.2
−0.8
−0.4
0
0.4
0.8
1.2

Fig. 19 Change in surface fluxes HadAM3 - HadAM3-R (Wm^{-2})

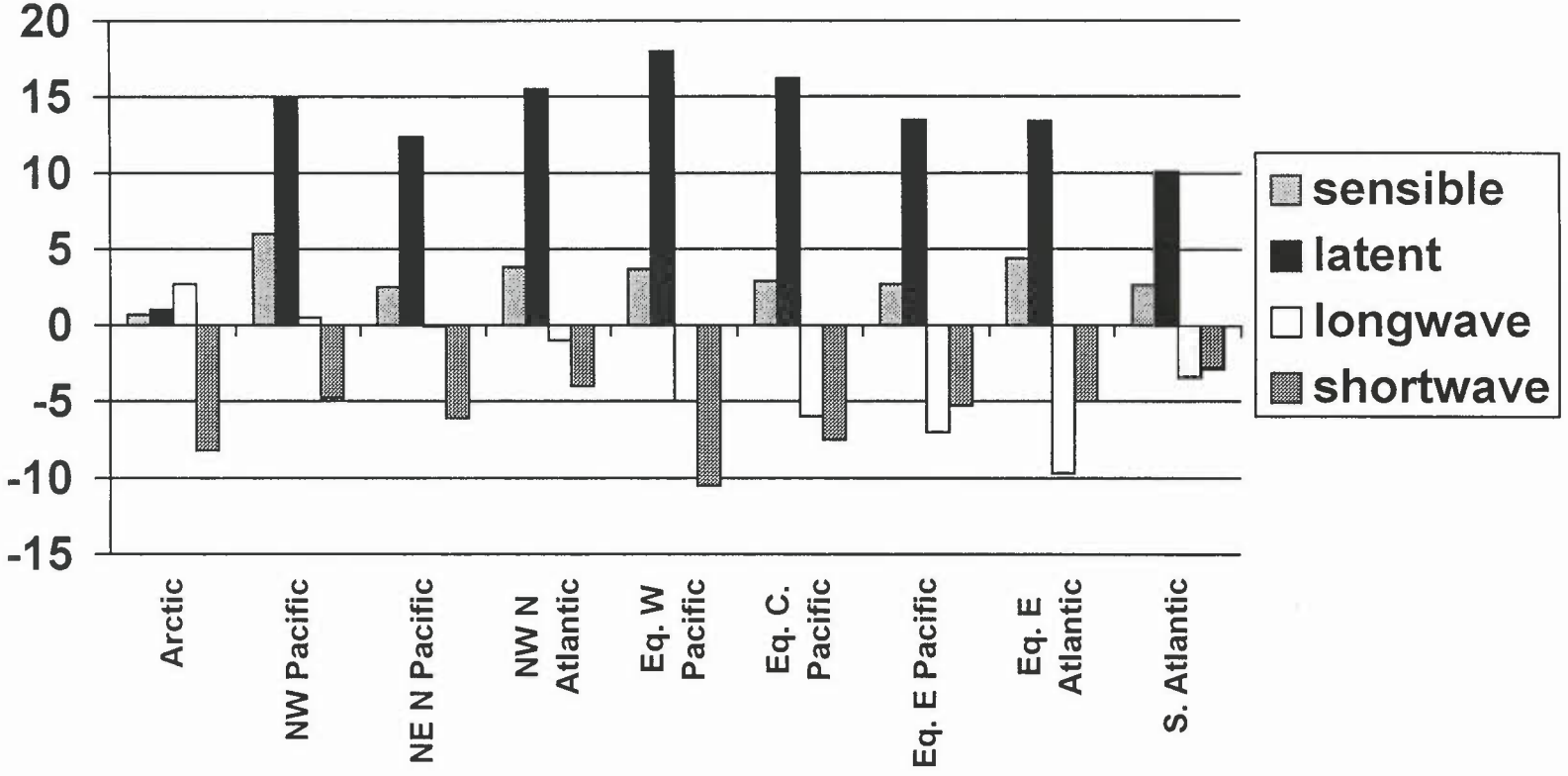

Fig 20

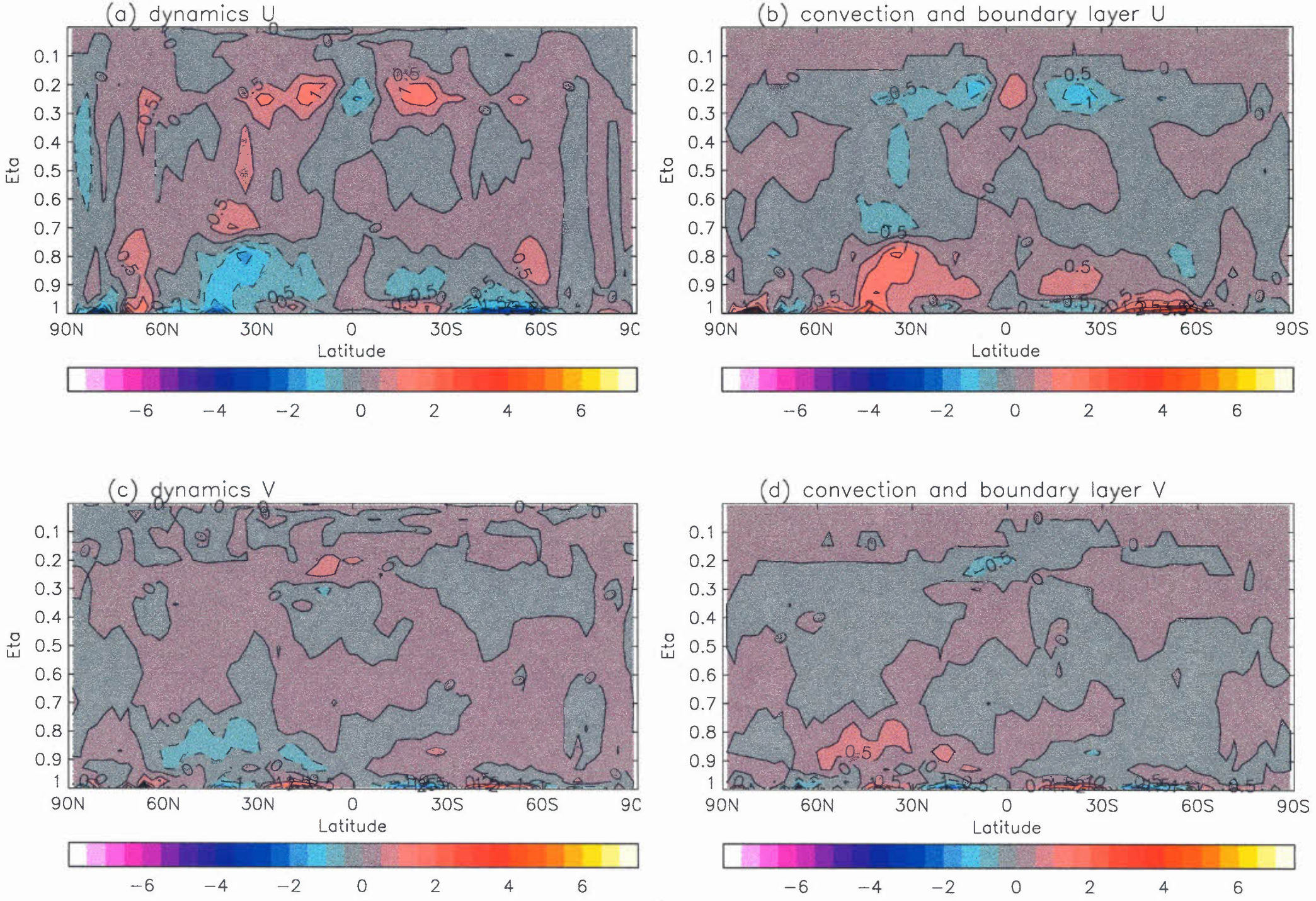
(a) dynamics U
(b) convection and boundary layer U
(c) dynamics V
(d) convection and boundary layer V
Eta
0.1
0.2
0.3
0.4
0.5
0.6
0.7
0.8
0.9
1
90N
60N
30N
0
30S
60S
90S
Latitude
−6
−4
−2
0
2
4
6

Fig.21 TEM streamfunction and Theta

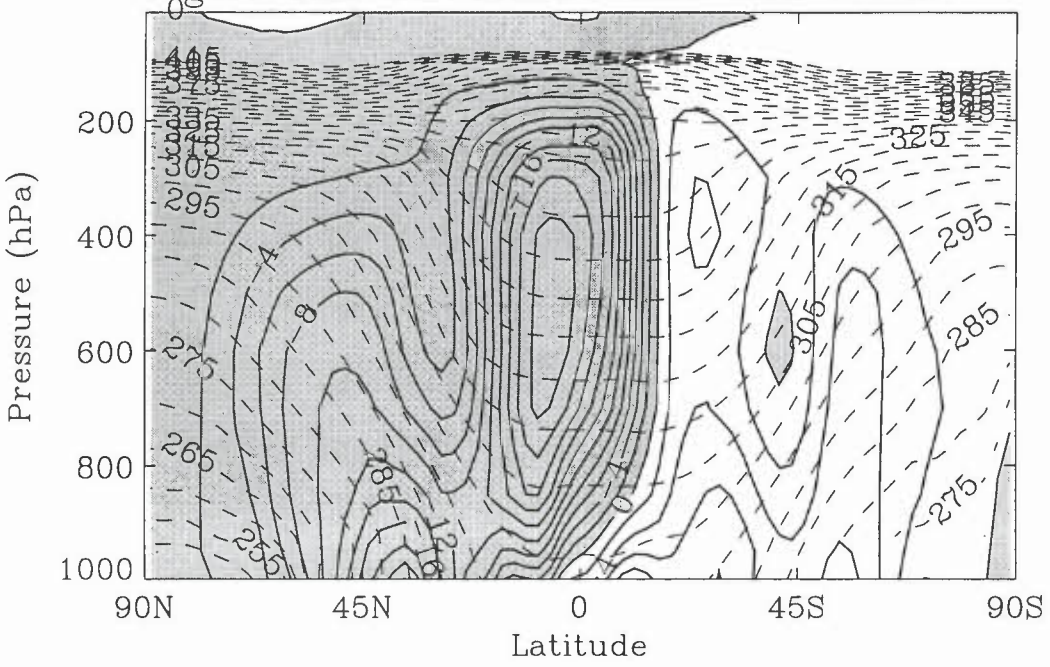

Fig.22 PMSL – impact of CMT

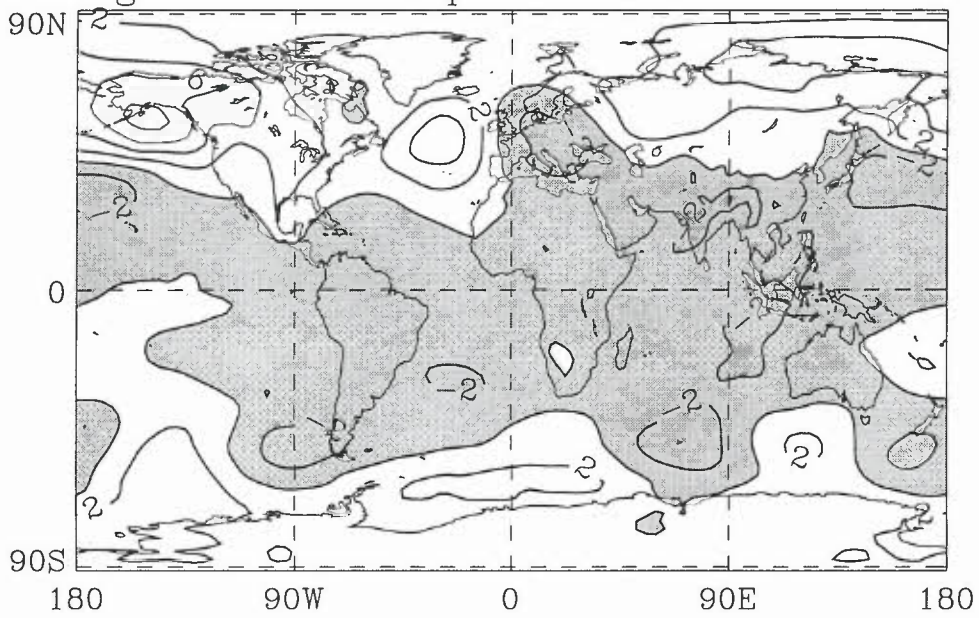

Fig. 23 Change in surface fluxes HadAM3-R - HadAM2b